Chapter 5

Studies of Iron doped InSb bulk and TM doped InSb films

This chapter is devoted to Fe concentration variation study in InSb bulk system and the comparative study of the transition metal doped InSb films. This chapter is divided in two parts.

In the first part study of Iron concentration variation in $In_{1-x}Fe_xSb$ bulk system is discussed. The effect of Iron concentration variation in bulk $In_{1-x}Fe_xSb$ is studied using XRD and Mossbauer spectroscopy. The results of these studies are elaborated.

In the second part various studies viz. structural, electrical, magnetoresistance, surface morphological and magnetic properties of thermally evaporated $In_{0.95}M_{0.05}Sb$ (M = Mn, Fe, Co and Ni) films are discussed.

5.1 Effect of Iron concentration variation in InSb bulk system

5.1.1 Introduction

The binary intermetallic compound InSb was synthesized in 1929 with a zinc blende structure [1]. But the In-Sb phase diagram was fully explained in 1952 [2]. Indium Antimonide (InSb) is an III-V group semiconductor with a band gap of ~ 0.17 eV at RT. It also has low effective mass (0.014 m_e) and high electron mobility at RT [3-4]. Due to it being low band gap semiconductor, it has been particularly attractive as a potential material for high performance devices, low temperature diodes, infrared detectors, IR laser devices, X-ray monochromation detector, optical-immersion lenses as well as magnetic sensors [5-8]. Hulme and Mullin [9] and Liang [10] *et. al.* worked on InSb with the material preparation, properties, and its basic applications. While Neuberger *et. al.* in 1965 [11] and in 1971 [12] summarized the key parameters of InSb.

The InSb is a narrow band gap III-V compound semiconductors. The E_0 gap is 235 meV at zero Kelvin and 172 meV at RT (300 K) [13] with the gap increasing nearly linearly from 300 K at 0.27 meVK^{-1} to about 232 meV at 77 K. This temperature range is of great interest. The gap is direct throughout this interval, means infrared emitters and detectors made from InSb tend to have high efficiency in this range.

InSb has the highest RT mobility (~ 7–8×10^4 cm^2 V^{-1}s^{-1}) amongst semiconductor. Since the signal response from a change in a transverse magnetic field in the Hall configuration is proportional to the square of the carrier mobility, so InSb thin films are widely used in magnetic sensors. InSb crystallizes in Zinc Blende structure (ZnS) with the F-43m space group that comprises two interpenetrating, face centered cubic sub-lattice relatively displaced a quarter of the primary cell body diagonal [14].

Pramila Mohan *et. al.* [15] reported the growth of the InSb bulk system, which is used for infrared device application. D. S. Maske *et. al.* [16] reported the Bi doped InSb bulk crystals prepared using Vertical Directional Solidification (VDS) technique and characterized for various studies. D. B. Gadkari *et. al.* [17] reported the characterization of p-type and n-type InSb bulk using VDS technique. Robert D. Grober *et. al.* [18] reported the time resolved photoluminescence studies of bulk InSb. A. A. Ebnalwaled *et. al.* [19] reported the growth of InSb crystal using the vertical Bridgeman technique and results is compared with previous studies. While in one of the study by A. A. Ebnalwaled [20] reported the hopping conduction and dielectric properties of InSb bulk crystals. Recently in 2016 K. E. Hnida *et. al.* [21] reported the electrochemically deposited nanocrystalline InSb with its electrical properties. There are many reports which show the various properties of pure InSb bulk. Apart from the studies of pure InSb there are many reports available with the inclusion of the various elements [22-27] in InSb bulk. D. B. Gadkari *et. al.* [22] reported the high mobility of InSb bulk with the doping of Tellurium. Shigeo *et. al.* [23] reported the thermo-electric properties and figure of merit of the Te doped InSb bulk. Manisha *et. al.* [24] reported the optical characteristics of dilute Nitride doped InSb bulk.

InSb, a zinc blende structure material can also behave like a dilute magnetic semiconducting material if doped with transition metal. A few studies like. V. A. Ivanov *et. al.* [25] reported the ferromagnetism in Mn doped InSb bulk. Kochura *et. al.* [26] concluded that the Mn doped InSb is a high temperature magnetic semiconductor due to the presence of nanosize MnSb precipitates. E. Lahderanta *et. al.* [27] reported the various studies of Mn doped InSb bulk magnetic semiconductor. In the literature survey a lot of reports are available on Mn doped InSb bulk system. But there are a few reports on other transition metal (as Fe, Co, Ni etc.) doped with InSb as a DMS material. Hence

it is thought to incorporate the Fe at different concentrations in InSb to observe the concentration variation effect in the bulk InSb system.

Nuclear probe methods such as Mossbauer Effect and perturbed angular correlations is utilized to study the defect properties in semiconductors **[28-29]**. Mossbauer spectroscopy is a very sensitive technique to find local probe interaction at the microscopic level in Iron rich alloys and compounds. The Mossbauer study of Iron rich InSb bulk ($In_{1-x}Fe_xSb$) is discussed. The Iron concentration is varied at the Indium site for x = 0.05, 0.10 and 0.20.

5.1.2 Experimental details

Highly pure (99.999 %, Alfa Aeser) Indium (In), Antimony (Sb) and Iron (Fe) is taken for making the un-doped and Fe doped InSb ($In_{1-x}Fe_xSb$) bulk. The concentration of Fe is varied from x = 0.00, 0.05, 0.10 and 0.20. Each sample of required amount is sealed in a small quartz tube at high vacuum of the order of 10^{-5} Torr. The vacuum sealed ampules is heated in the oxy-butane flame and cooled. This process is repeated many times to get homogeneity of the samples. The samples are quenched at RT in water and the ingots of bulk systems are ground to fine powder. A part of the powder is used for structural study and a part is used to prepare Mossbauer absorber. The structural study of the $In_{1-x}Fe_xSb$ (x = 0.00, 0.05, 0.10 and 0.20) bulk is characterized by powder X-ray Diffraction technique. The sample for Mossbauer absorber is evenly distributed on a one mm thick sheet of paper and the diameter of the absorber was ~ 1.2 cm. Before and after each run of spectra the velocity calibration is checked and recorded. The Mossbauer spectra are taken for the samples with a constant acceleration mode spectrometer whose line width is 0.31 mm/sec. All the Mossbauer spectra are recorded at RT.

5.1.3 Structural studies

The **figure 5.1** shows the comparative X-ray diffraction pattern of un-doped and Iron concentration variation of $In_{1-x}Fe_xSb$ (x = 0.00, 0.05, 0.10 and 0.20) bulk system. The peaks are indexed based on cubic structure (JCPDS file no. 89-4299) of InSb. It is observed that un-doped InSb is single phase face centered cubic structure with $F\bar{4}3m$ space group. The indexed peaks of un-doped InSb are at 23.7º, 39.3º, 46.4º, 56.7º, 62.4º and belong to hkl value of (111), (220), (311), (400) and (331) respectively.
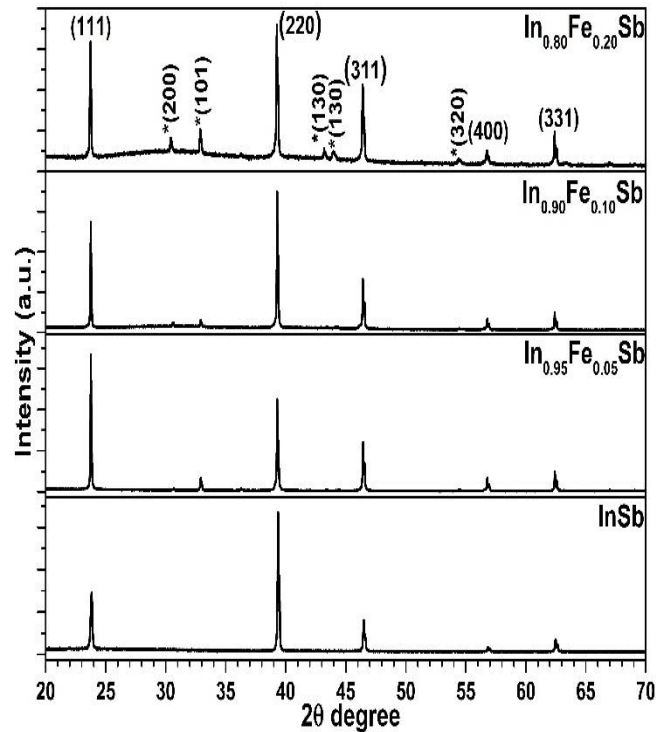
Figure 5.1: X-ray diffraction pattern of In$_{1-x}$Fe$_x$Sb (x = 0.00, 0.05, 0.10 and 0.20) bulk sample

When Fe is incorporated in InSb bulk system additional peaks at 30.4º (200), 32.9º (101), 43.1º (130) and 44.0º (211) are (**figure 5.1**) observed. These peaks are indexed with another phase of InSb and matches with the JCPDS data card no. 47-1502. The height of (111) peak in X-ray diffraction pattern for higher concentration of Fe *i.e.* $In_{0.80}Fe_{0.20}Sb$ shows a sharper peaks and small FWHM. The peak at (111) plane is found to be shifting towards lower 2θ value for Fe doped InSb as compare to un-doped InSb.

As the concentration of the Fe is made higher in InSb, the peaks are shifting more towards lower 2θ value.
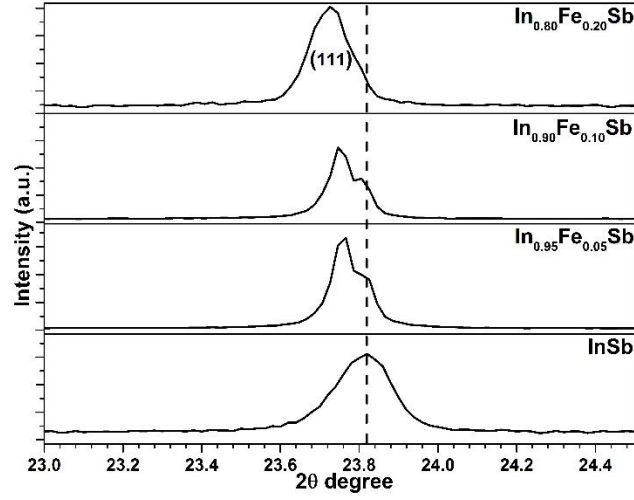
The (111) peak for In$_{1-x}$Fe$_x$Sb, for x = 0.00, 0.05, 0.10 and 0.20 is shown in **figure 5.2**. The peak of un-doped InSb bulk is used as a reference to compare the peak shift due to different reflections and hence to evaluate the microstructural parameters **[30]**. The shift of the peak due to the inclusion of Fe in InSb bulk depicts that the inter-planer spacing enhance with the increase in Fe concentration.

The crystallite size of In$_{1-x}$Fe$_x$Sb for x = 0.00, 0.05, 0.10 and 0.20 is calculated using William Hall equation. The William Hall plot is given in **figure 5.3**. The William Hall equation is given as **[31]**.

$$\beta Cos\theta = \frac{0.9\lambda}{L} + 4\,\mathcal{E}Sin\theta$$

Where β is full width at half maxima (FWHM) in radians, θ is Bragg angle in degree, λ is the wavelength of the source (1.54 Å), L is crystallite size and $\mathcal{E}$ is the strain. The strain is assumed to be uniform in all crystallographic directions, thus considering

the isotropic nature of the crystal, where all the material properties are independent of the direction along which they are measured [32].
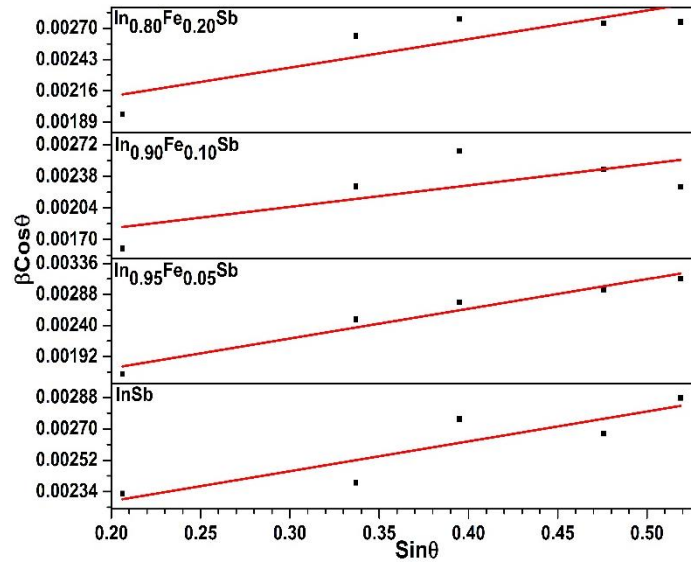

Figure 5.3: *William-Hall plot for $In_{1-x}Fe_xSb$ for x = 0.00, 0.05, 0.10 and 0.20 bulk system*

Sample composition $In_{1-x}Fe_xSb$	Structural parameters (nm)	
	Crystallite size	Strain ($\times 10^{-3}$)
x = 0.00	71.44	4.27
x = 0.05	168.42	11.47
x = 0.10	101.91	5.75
x = 0.20	85.54	6.15

Table 5.1: *structural parameters of $In_{1-x}Fe_xSb$ bulk for x = 0.00, 0.05, 0.10 and 0.20 respectively*

The observed crystallite size for un-doped and Fe doped InSb bulk range is ~ 71- 168 nm. The crystallite size for un-doped InSb is 71.44 nm. But when Fe is incorporated into the InSb system, the crystallite size increases to 168.2 for x = 0.05 and on further increase in Fe concentration the crystallite size decreases to 85.54 nm for x = 0.20. The obtained value of crystallite size and strain is given in **table 5.1**. The observed strain from the William Hall equation is in the range of ~ 4×10^{-3} nm for un-doped bulk InSb. But on incorporation of Fe in InSb the strain increases for x= 0.05 and on further increasing the Fe concentration from x= 0.10 to 0.20 the strain decreases to 5.75 nm for x = 0.10 and remains almost constant for x = 0.20.

5.1.4 Mössbauer study

Mossbauer study is done for the Fe doped InSb bulk alloy. The Mossbauer spectra are least squares fitted with a computer program named "Meerwal". The least square fitted Mossbauer parameters of the Fe doped InSb ($In_{1-x}Fe_xSb$, x = 0.05, 0.10 and 0.20) are given in **table 5.2**. The experimental error bar values are also given in the table. All the parameters are given with respect to Natural Fe. **Figure 5.4** shows the calibration spectra of natural Iron. The Mossbauer spectra of the Fe concentration variation in InSb are shown in **figures 5.5** to **5.7** for x = 0.05, 0.10 and 0.20 respectively.
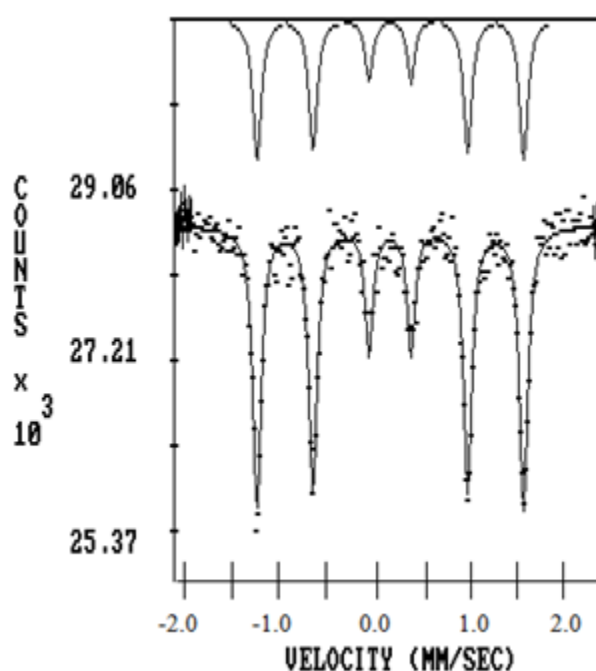
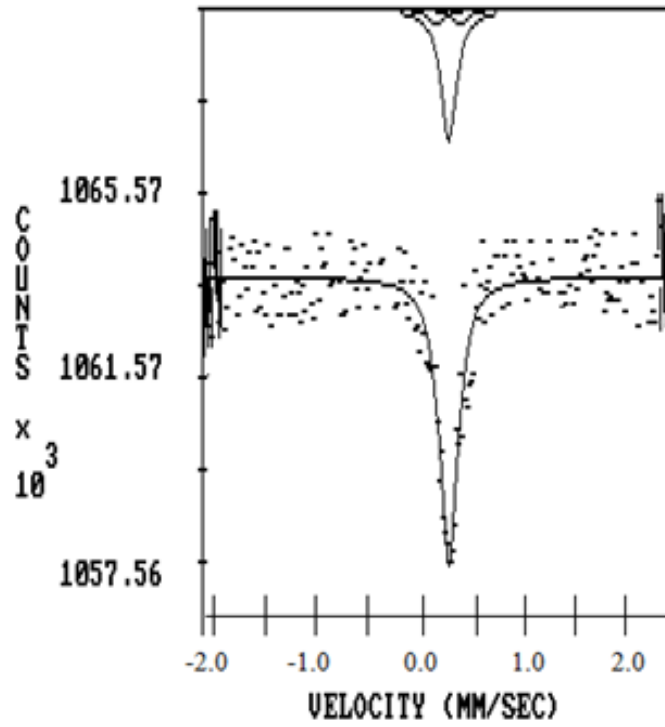**Figure 5.4:** *Calibration Mössbauer spectrum of Natural Fe*

Figure 5.5: Mössbauer spectrum of $In_{0.95}Fe_{0.05}Sb$

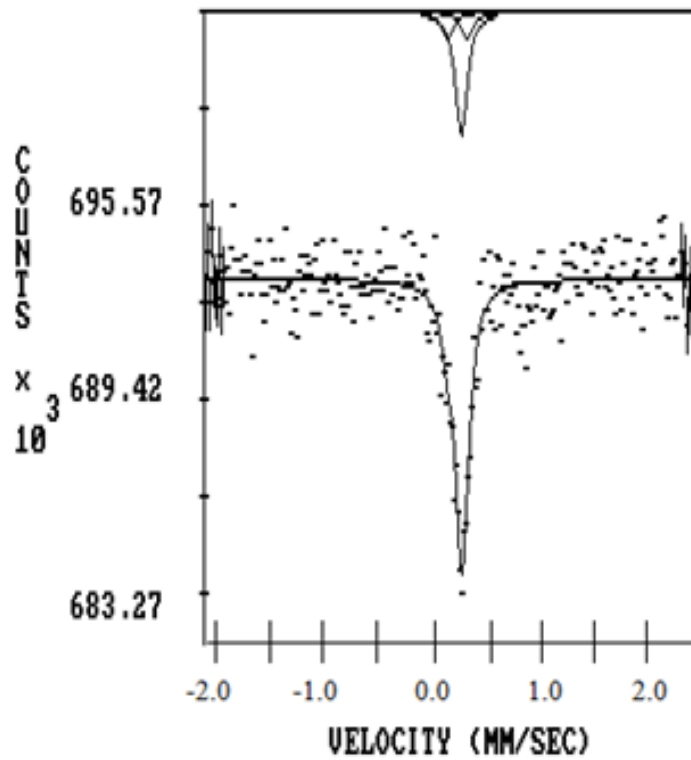*Figure 5.6: Mössbauer spectrum of $In_{0.90}Fe_{0.10}Sb$*

From the least square fitting of the data the values of Isomer shift, quadrupole splitting and area under the curve are evaluated using the velocity spectrum of the In_{1-}

$_x$Fe$_x$Sb (x = 0.05, 0.10 and 0.20) bulk system respectively. The best fit of the Mossbauer data is obtained when the In$_{1-x}$Fe$_x$Sb bulk system (**table 5.2**) is fitted for two different sites A and B. The Site A is a quadrupole site whereas site B is a singlet site. For the site A with the lowest concentration of Iron (x = 0.05) the value of isomer shift is the maximum which is 0.69 mm/sec.
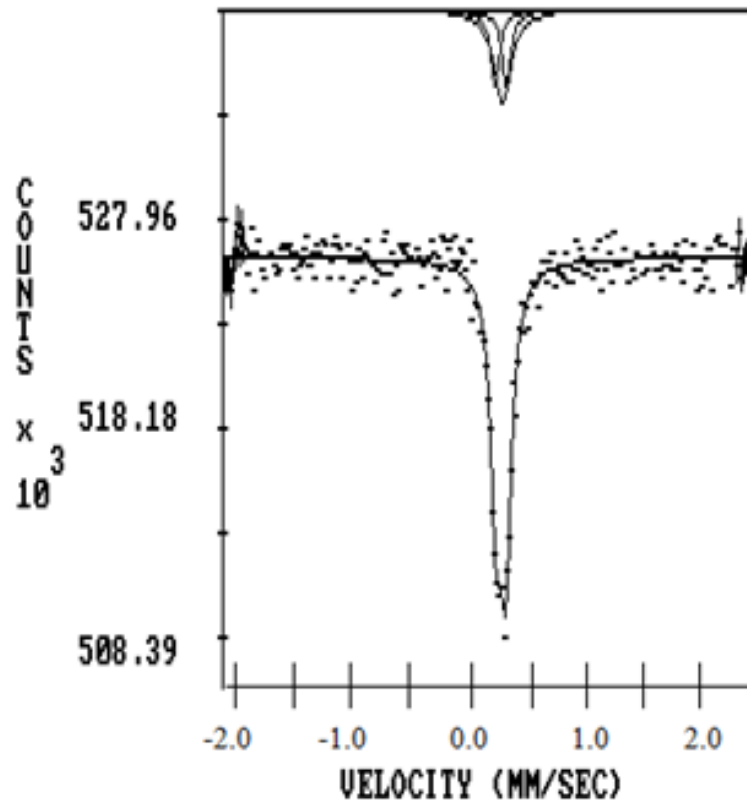

Figure 5.7: Mössbauer spectrum of In$_{0.80}$Fe$_{0.20}$Sb

Sample composition In$_{1-x}$Fe$_x$Sb	Quadrupole splitting (Q.S. ±0.02) (mm/sec)		Isomer shift (I.S. ±0.02) (mm/sec)		Area under the curve (%)	
	A	**B**	**A**	**B**	**A**	**B**
x = 0.05	0.89	---	0.69	0.42	22.0	78.0
x = 0.10	0.70	---	0.56	0.44	31.5	68.5
x = 0.20	0.36	---	0.42	0.45	39.2	60.8

Table 5.2: Mossbauer parameters of In$_{1-x}$Fe$_x$Sb (x = 0.05, 0.10 and 0.20)

With increasing the Iron concentration the isomer shift of site A decrease from 0.69 to 0.56 and to 0.42 mm/sec for x = 0.10 and x = 0.20 respectively. But the value of isomer shift for site B remains approximately constant.

The quadrupole splitting value for site A is 0.89 mm/sec for x = 0.05 but the quadrupole splitting decreases from 0.70 to 0.36 when the Fe concentration is increased from x = 0.10 to 0.20 in $In_{1-x}Fe_xSb$ bulk system. The population of site A for x = 0.05 is minimum (22 %) and it is maximum for site B (78 %) respectively. As the Fe concentration is increased from x = 0.10 to x = 0.20 the population for site A increase from 31.5 to 39.2 % with the increase in Iron concentration while that of site B the population decreases from 68.5 to 60.8 %.

The singlet site B is attributed to the cubic phase of InSb in which Fe is going to the substitutional In site in InSb. The site A seems to be due to another phase of InSb which is non-cubic. Although the value of QS is not very large still a quadrupole splitting is observed in this case indicating a distorted cubic phase.

This value of QS decreases with the increase in Iron concentration in InSb. At x = 0.20, there is a sharp decrease in the QS with a value of 0.36 mm/sec. This depicts that the site A is going towards more and more symmetry on Fe doping. The XRD also supports this argument which clearly shows two phases of InSb on doping with Fe. No magnetic interaction is observed even when the concentration of Fe is increased up-to x = 0.20. This show that even at this higher concentration up to x = 0.20, Fe can be incorporated in InSb without Iron forming Fe clusters or giving rise to any magnetic interaction.

The decrease in Isomer shift for site A indicates that the electron density at the Fe nucleus decrease with the increase in Fe concentration. Also predominantly Fe is in +3 charge state in InSb. The IS at site B is almost constant at ~ 0.44 mm/sec. This shows that the environment around the Fe nucleus remains almost same for this site which is cubic in nature.

5.2 Comparative study of transition metal doped InSb films

5.2.1 Introduction

The InSb has various applications in the field of semiconductor physics **[3-27]**. The InSb films are grown using different film growth techniques, on different substrates and in a different environment for various application purposes. Different techniques such as molecular beam epitaxy (MBE) **[33-35]**, metalorganic magnetron sputtering **[7]**, metalorganic vapor phase epitaxy **[36]**, and Vertical Bridgemen Technique **[37]** have been used to grow InSb films. The films can be fabricated on InSb, GaSb, GaAs or InAs substrates. But this method is not preferred due to the low resistance of the substrate. Instead, GaAs and Si substrates are more used even though there is a significant lattice mismatch between substrate and epitaxial layer (lattice mismatch 14.6 % between InSb and GaAs, and 19.3% between InSb and Si) **[38-39].** Moreover, the advantage of growing InSb on Si is the availability of high quality and large size Si substrates. There are some studies in the direct growth on Si substrate **[3, 40-41]**.

In one of the work by Mori *et. al.* **[42]**, InSb films is grown on Si (111) substrate with In-Sb bilayer at high growth temperature. The In-Sb bilayer is prepared by the adsorption of one monolayer Antimony atoms onto Indium induced surface reconstruction on a Si (111) substrate. The influence of the substrate temperature of first layer deposition on the two step growth procedure is studied. The RT electron mobility of the InSb film on Si (111) substrate at the 420 ºC with an In-Sb bilayer is about 2000 cm^2/Vs.

The dilute magnetic semiconductors are of II-VI, III-V, IV-IV types. The studies of the DMS have concentrated most extensively on II-VI semiconductors, such as CdTe and ZnSe, in which the valence of the cations matches that of the doped magnetic ions.

This phenomenon makes these DMS relatively easy to prepare in both bulk form and thin epitaxial layers.

Indium Antimonide doped with Manganese is produced by using various methods. The single crystal of Mn doped InSb is grown using the Czochralski method [43-45] with manganese concentration up to 5×10^{18} - 1×10^{19} cm^{-3} [44]. The first attempt to grow InSb films with heavily doped Mn using MBE technique is described by D. L. Martin *et. al.* [46]. This Mn doped InSb film is grown using a substrate temperature of 300 and 360 $^{\circ}$C. In some other studies the low temperature MBE with a substrate temperature of 170 $^{\circ}$C is used to avoid forming of precipitation phase and to raise the Manganese solubility in InSb [47-51]. The doping of Mn in InSb ($In_{1-x}Mn_xSb$) shows ferromagnetism with $T_c \sim 8$ K for x = 0.028 [49] and for x = 0.10, T_c is 20 K [51].

The value of $T_c \sim 130$ K is obtained for bulk InMnSb which is synthesized using controlled ambient annealing technique [52]. The value of T_c above RT is observed in InMnSb films grown by pulse laser deposition [53] and liquid phase epitaxy [54] techniques.

There are lots of reports available in the literature which discusses about ferromagnetism in Mn doped InSb at higher and lower Mn concentrations, below RT or above RT which are prepared using various techniques in the form of the bulk and thin films. There are no reports of magnetic studies of transition metal (except Mn) doped InSb films which grow on Silicon substrate. In the present work, un-doped InSb and transition metal doped $In_{0.95}M_{0.05}Sb$ films grown on Si substrate using thermal evaporation technique are studied. Here the doped transition metals (M) are Fe, Co, Ni, and Mn. To observe the effect of different transition metals in InSb film system the various studies as structural, electrical, magneto-transport, surface morphological and magnetic studies are done.

5.2.2   Experimental details

Highly pure (99.999 %, Alfa Aeser) Indium, Antimony and transition metals Iron (Fe), Cobalt (Co), Nickel (Ni) and Manganese (Mn) is taken for making the un-doped InSb and TM doped InSb ($In_{0.95}M_{0.05}Sb$, M = Mn, Fe, Co and Ni) bulk alloy. Each sample of required amount is sealed in a small quartz tube at high vacuum of $>10^{-5}$ Torr. The vacuum sealed ampule is heated in the oxy-butane flame and cooled. This process is repeated many times to get homogeneity of the samples. The samples are quenched at RT in water and the ingots of bulk alloy are ground to fine powder. This powder is used to grow the un-doped and transition metal doped $In_{0.95}M_{0.05}Sb$ (M = Fe, Co, Mn and Ni) films. The details of thin film growth technique (thermal evaporation technique) are given in chapter 2. The thickness of the film is 500 nm, measured with fizaeu fringes technique.

The structural studies of alloy films are characterized by Grazing angle X-ray Diffraction (GAXRD) technique using Bruker D8 Advance X-ray diffractometer. The X- rays are produced using a sealed tube with the 0.154 nm (CuK_α) wavelength. The X-rays are detected using a fast counting detector based on silicon strip technology (Bruker LynxEye detector). This XRD pattern is monitored at RT with a constant rate of 0.05 degree/6 s at grazing angle (α) of 0.5°. The resistivity measurement is done on the films having control doping of different transition metals *i.e.* $In_{0.95}M_{0.05}Sb$ (M = Fe, Co, Mn and Ni), using Physical property measurement system (PPMS) for the temperature range of ~ 20 K to 370 K. For this study Indium is used to make the contact. The details of the PPMS system are discussed in chapter 2. The sample surface is analyzed using Atomic Force Microscope (AFM) from Digital Instruments (Nanoscope III) with Si_3N_4 tips under ambient conditions in the contact mode at RT. It provides high resolution surface micrographs. Magnetic imaging of sample surface as a function of different transition

metal is carried out by a magnetic force microscope (MFM) from the Nano magnetic instrument at RT. AFM and MFM are employed to spatially probe the structure of the sample surfaces and distribution of the local magnetic field.

5.2.3   Structural studies

Structural characterization of pure Indium Antimonide (InSb) and $In_{0.95}M_{0.05}Sb$ (M = Fe, Mn, Ni and Co) film is done using Grazing Angle X-ray diffraction technique with CuK_α radiation. The comparative X-ray diffraction pattern of un-doped InSb bulk (taken before film preparation), InSb un-doped film and $In_{0.95}M_{0.05}Sb$ (M = Fe, Mn, Ni and Co) films are shown in **figure 5.8**.
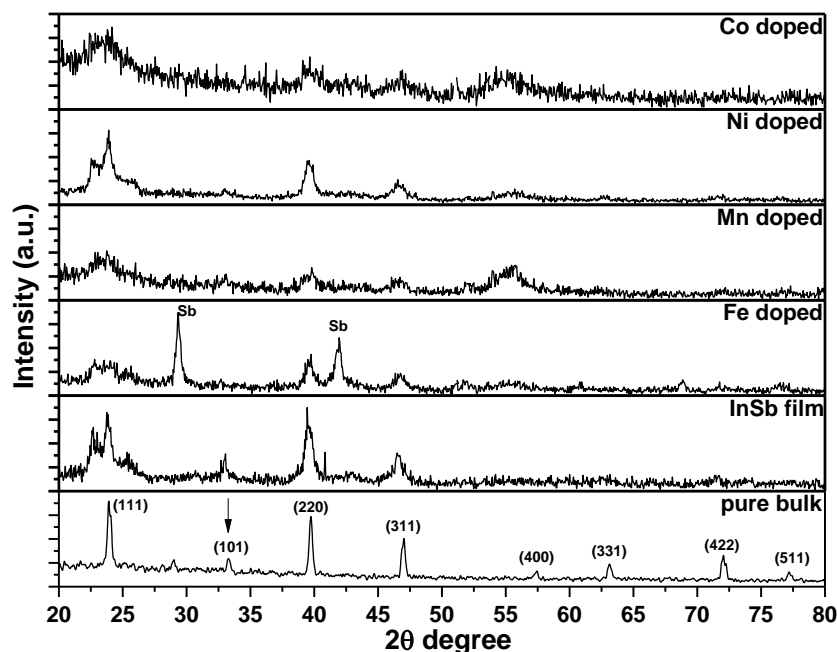
Figure 5.8: Comparative XRD spectra of un-doped InSb bulk, un-doped InSb film and $In_{0.95}M_{0.05}Sb$ (M = Mn, Fe, Co and Ni) films

In the diffraction pattern the observed peak positions at 23.9º (111), 39.7º (220), 47.0º (311), 57.5º (400), 63.1º (331), 71.9º (422) and 77.1º (511) is well indexed with the face centered cubic structure and $F4\overline{3}m$ space group of InSb compound phase which matches with the JCPDS data card no 73-1985. While in $In_{0.95}Fe_{0.05}Sb$ film, reflections at the 29.3º and 42º is also observed. This reflection seems to be due to the Antimony

rhombohedral structure and matches with the JCPDS data card no. 05-0592. In this diffraction pattern no peak/peaks of low concentration transition metal dopant Fe, Co, Mn and Ni or its phases with In or Sb are observed. It is also observed from the XRD spectra that the un-doped and TM doped films are nano-crystalline in nature.

5.2.4 Electrical Studies

The temperature dependent resistivity (DC resistivity) of transition metal doped InSb films is done using Quantum Design Physical property measurement system (PPMS) system.
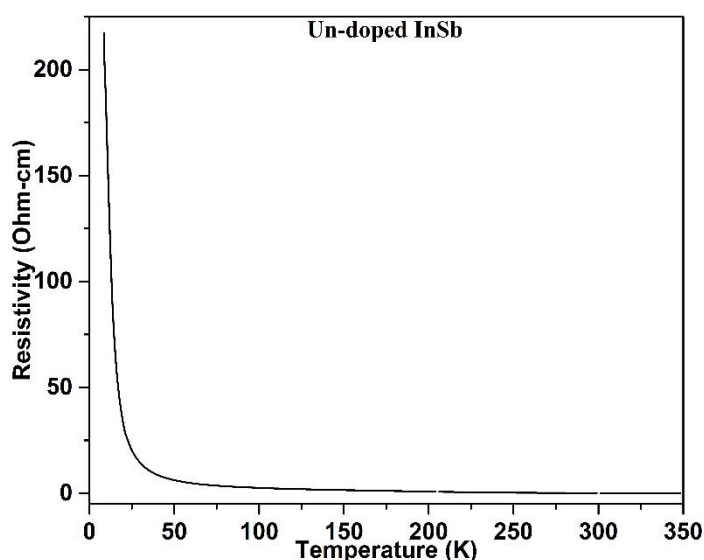
Figure 5.9(a): *Resistivity versus temperature spectra of un-doped InSb film*
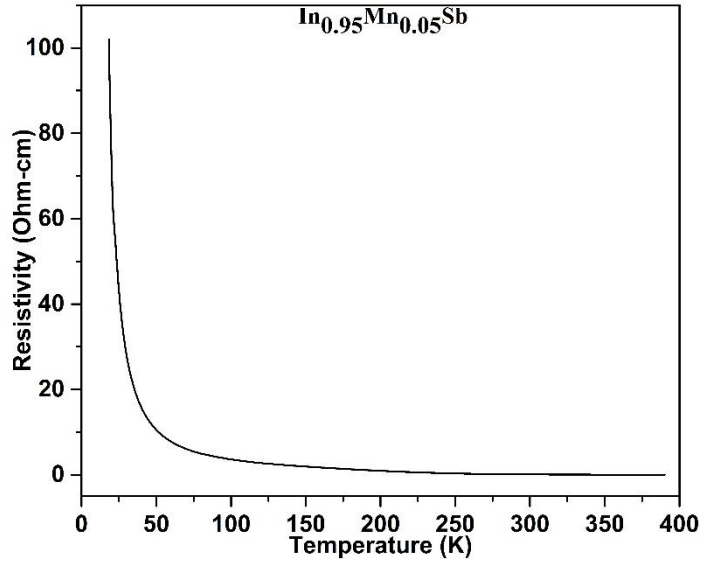
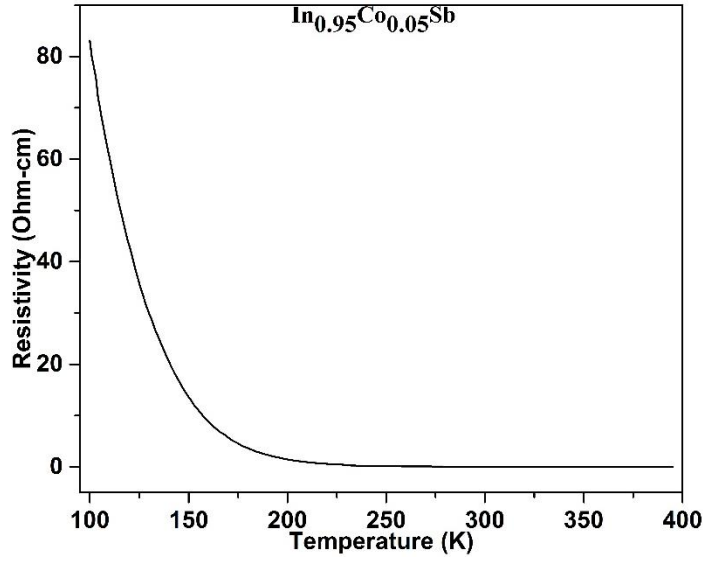*Figure 5.9(b): Resistivity versus temperature spectra of $In_{0.95}Mn_{0.05}Sb$ film*
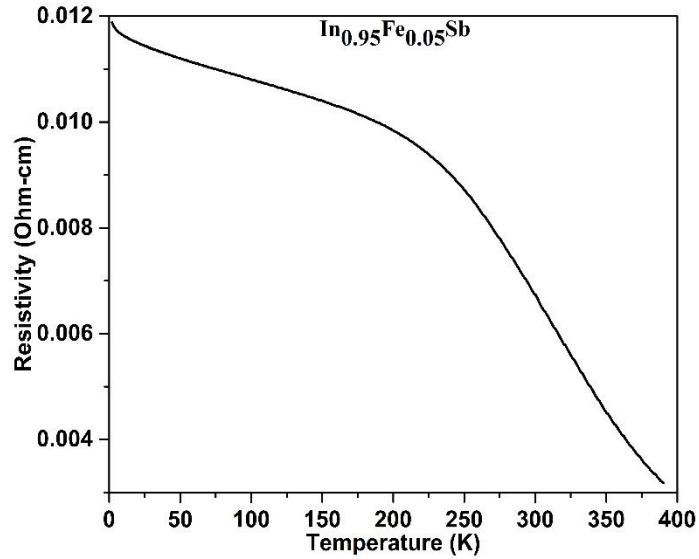
Figure 5.9(c): Resistivity versus temperature spectra of $In_{0.95}Fe_{0.05}Sb$ film

The resistivity as a function of temperature at zero field is shown in **figure 5.9(a-e)**. The resistivity of un-doped and doped films is taken in the temperature range of ~ 20-370 K in zero magnetic field. The resistance of all the films is of the order of milli-Ohms to few Ohms. The resistivity of all films (un-doped and transition metal doped) decreases with the increase in temperature, which depicts the semiconducting nature of films **[55]**.

Figure 5.9(d): *Resistivity versus temperature spectra of In$_{0.95}$Co$_{0.05}$Sb film*
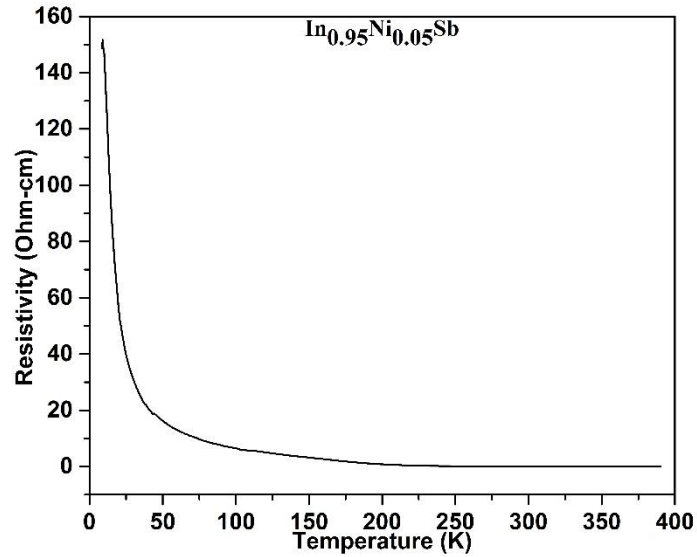
Figure 5.9(e): *Resistivity versus temperature spectra of In$_{0.95}$Ni$_{0.05}$Sb film*

It is observed that in transition metal Mn, Ni and Co doped InSb films, the resistivity of the film increases. But the Iron doped InSb film shows that the resistivity decreases as compare to un-doped film due to the inclusion of Fe. The increasing resistivity order for Un-doped and transition metal doped films is In$_{0.95}$Fe$_{0.05}$Sb < Un-doped InSb < In$_{0.95}$Mn$_{0.05}$Sb < In$_{0.95}$Ni$_{0.05}$Sb < In$_{0.95}$Co$_{0.05}$Sb respectively.

The activation energy is calculated using the Arrhenius equation. Arrhenius equation is given as

$$R(t) = R_0 \exp(E_a/K_b T)$$

Where R(t) is resistivity at temperature T, E_a is the activation energy and K_b is the Boltzmann constant. The Arrhenius plot to obtain activation energy is shown in **figure 5.10(a-e)**.
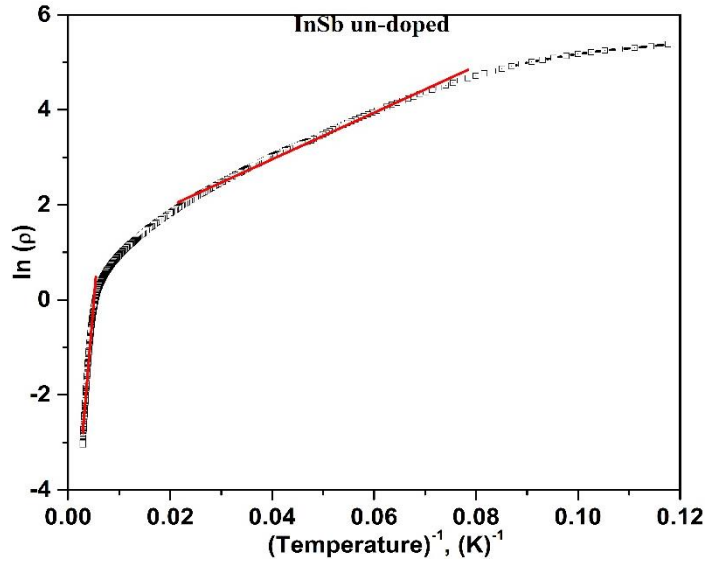

Figure 5.10(a): *The Arrhenius plot for un-doped InSb film. The solid red line is the linear fit of the data*
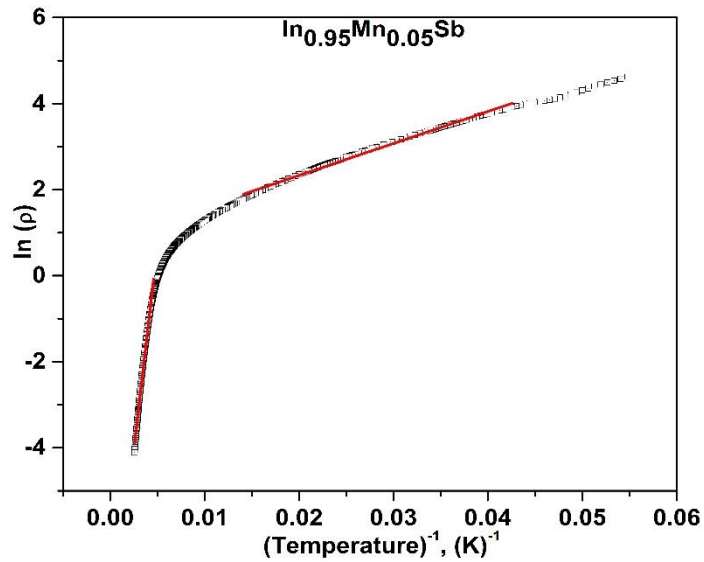

Figure 5.10(b): *The Arrhenius plot for $In_{0.95}Mn_{0.05}Sb$ film. The solid red line is the linear fit of the data*

The activation energy is found out in two different temperature regions near 300 K and near 100 K. It is observed from **figure 5.10(a-e)** that due to incorporation of transition metal in InSb films the activation energy (E_a) increases except for $In_{0.95}Fe_{0.05}Sb$ film

with respect to un-doped InSb film. In the Fe doped InSb film the activation energy decreases as compared to the un-doped InSb film for both higher and lower temperature range.
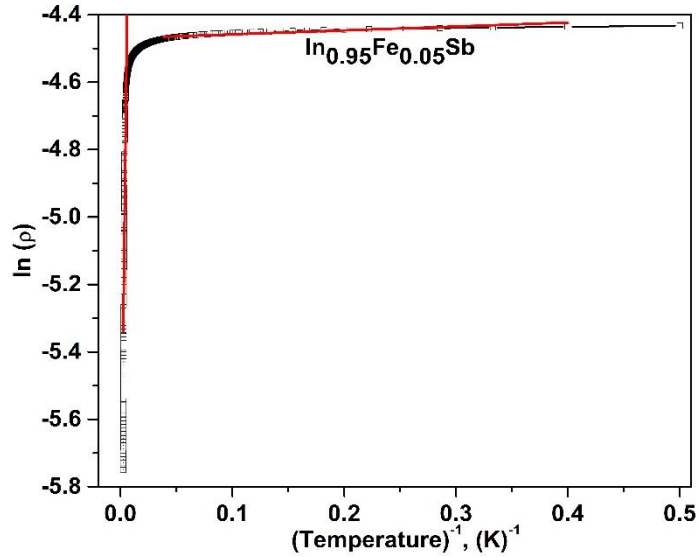

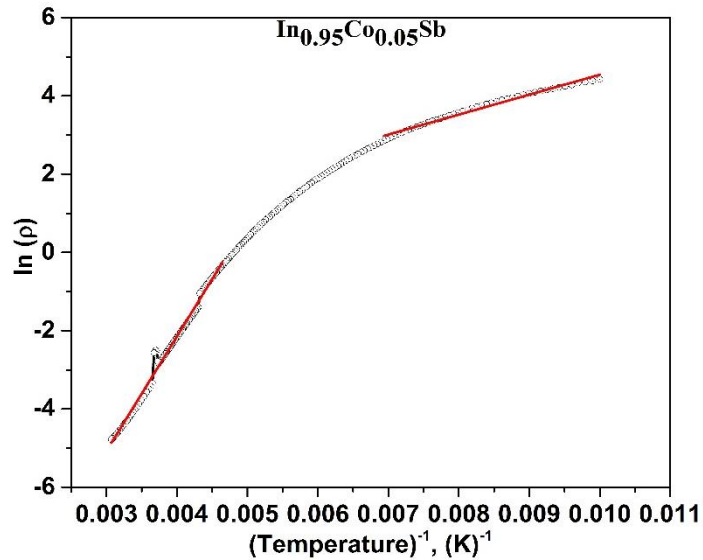**Figure 5.10(c):** *The Arrhenius plot for In$_{0.95}$Fe$_{0.05}$Sb film. The solid red line is the linear fit of the data*

Figure 5.10(d): *The Arrhenius plot for In$_{0.95}$Co$_{0.05}$Sb film. The solid red line is the linear fit of the data*

The value of activation energy is found to be 0.01- 6.4 meV in the temperature region ~ 100 K and it is 24.0 -169.3 meV for the temperature region ~ 300 K. The calculated activation energy from Arrhenius plots is given in **table 5.3**.
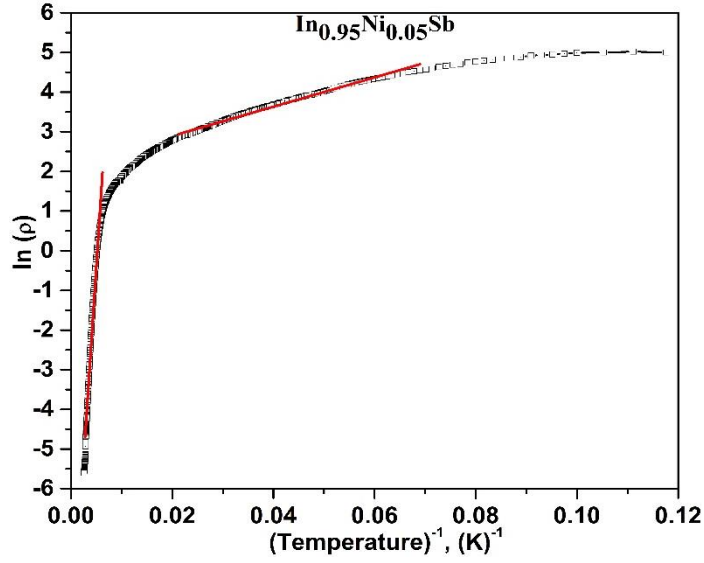
Figure 5.10(e): The Arrhenius plot for In$_{0.95}$Ni$_{0.05}$Sb film. The solid red line is the linear fit of the data

Usually in order to explain the low temperature conduction mechanism, the hopping conductivity in the disordered systems is understood by a variable range hopping mechanism (VRH) as suggested by Ambegaokar *et. al.* [56].

His idea is based on a model in which charge is transported by thermally assisted hopping of electrons between localized states, which are randomly distributed at energy and positions. The VRH mechanism is governed by [57].

$$\rho\,(t) = \rho_0 \exp\,(T_0/T)^{1/4}$$

Where ρ_0 and T_0 denote the material parameters and $T_0 = [1.5/\alpha^3\,N(E)]/K_b$, where $N(E)$ is the density of the state at Fermi level and α denotes the rate of fall-off of the envelop of the electron wave function. The plotted normalized resistivity ($\ln\rho$) as a function of $(1/T)^{1/4}$ is shown in **figure 5.11(a-e)**.

These plots are straight line and it depicts both the experimental and fitted values for both the temperature range 100-150 and 210-350 K. The value of T_0 is obtained from the slope of the fitted straight line (red lines in **figure 5.11(a-e)**). The calculated value of T_0 for both the temperature range is shown in **table 5.4**. It is noted that the hopping

conductivity mechanism fits very well in this system for the two different temperature ranges of 100-150 K and 210-350 K respectively.
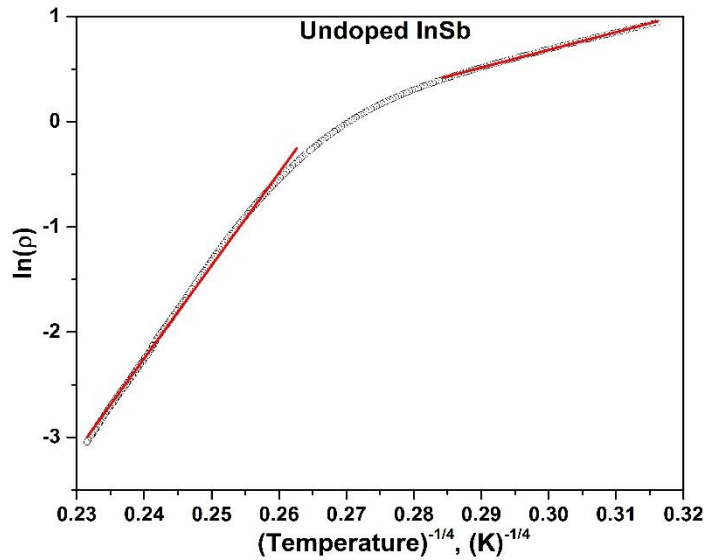

Figure 5.11(a): Temperature dependence of resistivity ρ(T) measured for un-doped InSb film, by the relation based on the three-dimensional Mott's variable range hopping conduction (3-D VRH), using equation, $\rho \propto \exp (T_0/T)^{1/4}$. The solid red lines are the linear fit of the data

Composition	Resistivity (Ohm-cm)	Activation Energy (meV)	
	At temperature 300 K	Fitted for low temperature region ~ 100 K	Fitted for high temperature region ~ 300 K
InSb	0.106	4.2	109.5
$In_{0.95}Mn_{0.05}Sb$	0.099	6.4	163.1
$In_{0.95}Fe_{0.05}Sb$	0.007	0.01	24.0
$In_{0.95}Co_{0.05}Sb$	0.014	4.3	169.3
$In_{0.95}Ni_{0.05}Sb$	0.024	3.1	167.0

Table 5.3: Activation energy calculated from electrical studies for un-doped InSb and $In_{0.95}M_{0.05}Sb$ (M = Mn, Fe, Co and Ni) film

Composition	$(T_0)^{1/4}$ values calculated from VRH mechanism $(K^{1/4})$	
	Temperature range 100-150 K	Temperature range 210-350 K
InSb	16.83	88.24
$In_{0.95}Mn_{0.05}Sb$	20.34	103.75
$In_{0.95}Fe_{0.05}Sb$	01.26	39.56
$In_{0.95}Co_{0.05}Sb$	59.63	170.49
$In_{0.95}Ni_{0.05}Sb$	22.55	140.14

Table 5.4: Electrical studies parameters calculated from VRH mechanism for un-doped InSb and $In_{0.95}M_{0.05}Sb$ (M = Mn, Fe, Co and Ni) film
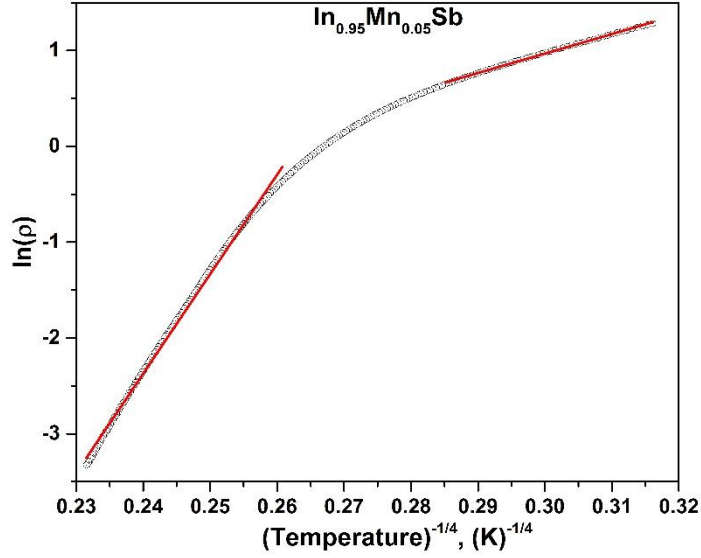
Figure 5.11(b): *Temperature dependence of resistivity ρ(T) measured for $In_{0.95}Mn_{0.05}Sb$ film, by the relation based on the three-dimensional Mott's variable range hopping conduction (3-D VRH), using equation, $\rho \propto exp\ (T_0/T)^{1/4}$. The solid red lines are the linear fit of the data*
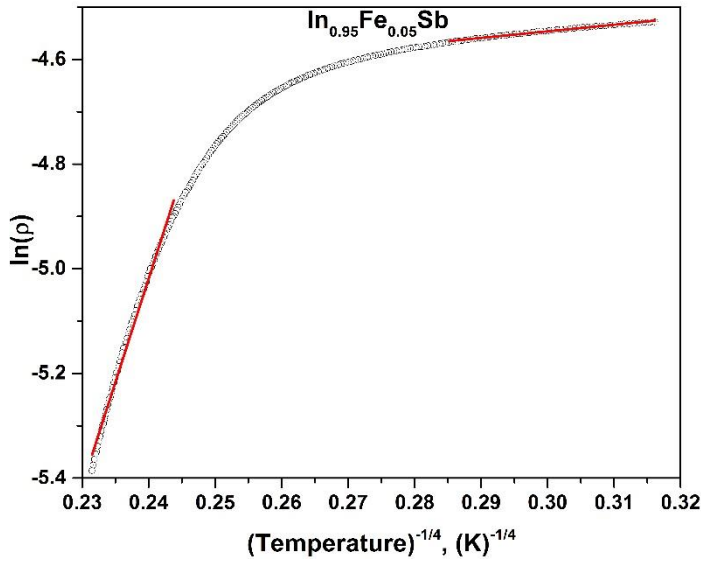

Figure 5.11(c): *Temperature dependence of resistivity ρ(T) measured for $In_{0.95}Fe_{0.05}Sb$ film, by the relation based on the three-dimensional Mott's variable range hopping conduction (3-D VRH), using equation, $\rho \propto exp\ (T_0/T)^{1/4}$. The solid red lines are the linear fit of the data*

It is observed that the value of T_0 for both the temperature ranges with the doping of transition metal increases except for Fe doping as compare to un-doped film. The value of T_0 for $In_{0.95}Fe_{0.05}Sb$ decreases as compared to un-doped film for both the temperature range. The value of T_0 is maximum for $In_{0.95}Co_{0.05}Sb$ and its minimum for $In_{0.95}Fe_{0.05}Sb$ film. This suggests that the density of state at the Fermi level decreases

due to doping of Co, Mn and Ni but it increases for Fe doped InSb film. The increasing order of density of states for un-doped and transition metal doped films are "Co doped < Ni doped < Mn doped < un-doped < Fe doped".
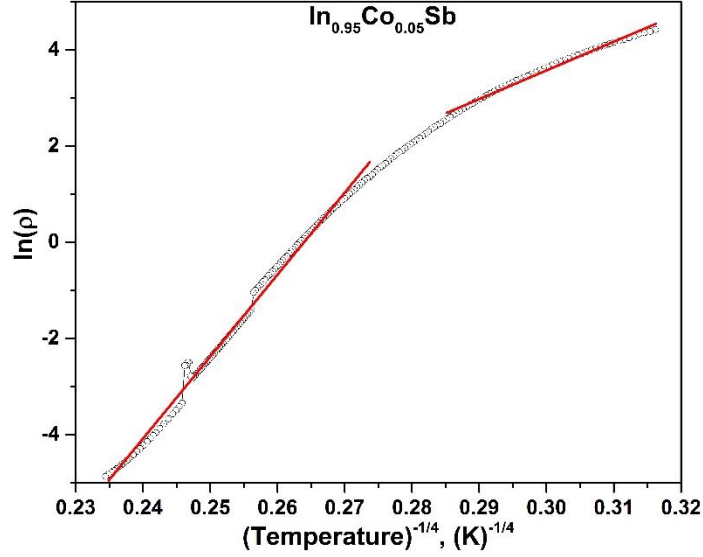

Figure 5.11(d): *Temperature dependence of resistivity ρ(T) measured for In$_{0.95}$Co$_{0.05}$Sb film, by the relation based on the three-dimensional Mott's variable range hopping conduction (3-D VRH), using equation, ρ ∝ exp (T$_0$/T)$^{1/4}$. The solid red lines are the linear fit of the data*

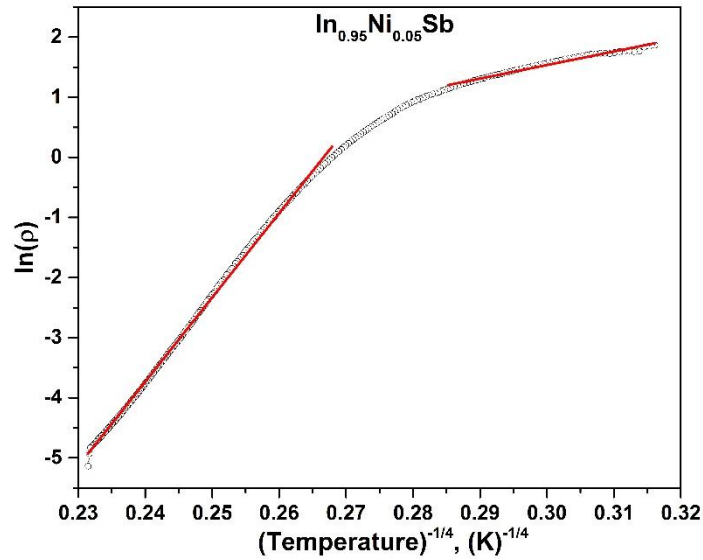**Figure 5.11(e):** *Temperature dependence of resistivity ρ(T) measured for In$_{0.95}$Ni$_{0.05}$Sb film, by the relation based on the three-dimensional Mott's variable range hopping conduction (3-D VRH), using equation, ρ ∝ exp (T$_0$/T)$^{1/4}$. The solid red lines are the linear fit of the data*

5.2.5   Magnetotransport studies

The magnetoresistance effect was discovered by Lord Kelvin in 1856, who was examining the resistance of Iron sample. The magnetoresistance appears in models with more than one carrier, and its high field behavior depends on the topology of the Fermi surface [58]. The change in electrical resistance 'R' of a conducting material subjected to a magnetic field 'H' applied perpendicular to the current is known as magnetoresistance. The magnetoresistance ratio is defined as $\Delta R/R$ and given by

$$\frac{\Delta R}{R} = \frac{R(H) - R(0)}{R(0)}$$

Where R(H) is the resistance at applied field and R(0) is the zero field resistance. Magnetoresistance sensors are extensively used as readout devices for magnetic bubble memories (measuring the magnetic field from the magnetic strip on a credit card).

The magnetoresistance effect is a function of the free carrier mobility due to this high carrier mobility, intermetallic compound semiconductors have been widely studied for the use as magnetoresistors. The InSb has wide attention due to its highest mobility (70×10^4 am^2/V. sec) of the more common single crystal intermetallic semiconductors [59]. Also, crystalline semiconductors have higher carrier mobility than their polycrystalline counterparts. Many researchers have done their work on intermetallic film semiconductor films [60-63].

For the magnetotransport study of transition metal doped InSb film magnetoresistance measurement is done using four point probe using a superconducting magnet in the PPMS system at different temperatures. The details of PPMS system are given in chapter 2. The applied magnetic field is perpendicular to the current in the specimen. The magnetoresistance ratio ($\Delta R/R$) versus magnetic field for the un-doped

and $In_{0.95}M_{0.05}Sb$ (Mn, Fe and Ni) films at different temperature is shown in **figure 5.12(a-d)**.
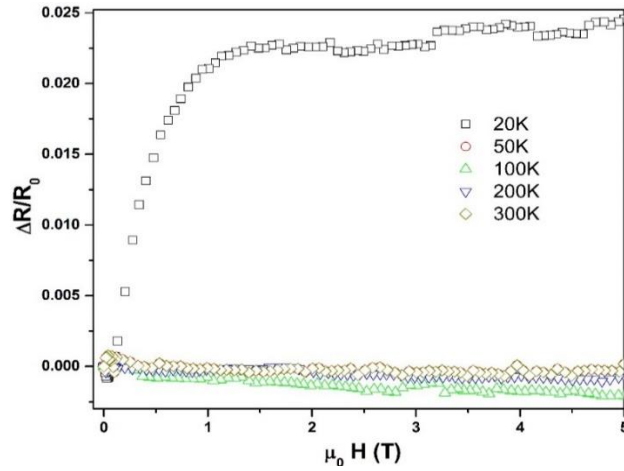

Figure 5.12(a): *Magnetoresistance ratio ($\Delta R/R$) versus magnetic field of the un-doped InSb film at different temperature*

The un-doped InSb film shows the 2.4 % variation in resistance at 20 K for an applied field of 5 tesla (**figure 5.12(a)**). For higher temperatures exceeding 20 K the magnetoresistance ratio is almost constant and there is no change in the magnetoresistance ratio till 300 K for un-doped InSb film. At 20 K the MR value increases with the applied field and saturates when the applied field is increased beyond 1.5 tesla. This seems to be due to the less Kinetic energy of the electrons at this low temperature. But with the increase in temperature till RT the magnetoresistance ratio is almost constant, *i.e.* there is no change in resistance with applied magnetic field. As at higher temperatures the electrons are more mobile and randomly oriented. Also, the surface to volume ratio of the films is very high. Hence the mobility of electrons is also high, resulting in almost no variation in the MR ratio with the increase in applied field. To have a magnetoresistance effect, there are two forces which play a major role. The externally applied field which tries to align the electron spins in the direction of the field. But at higher temperature the kinetic energy of the electrons becomes more resulting in

random alignment of the spins. This compensates the external magnetic field effect showing no changes in MR. To compensate the high temperature effect and to see the change in magnetoresistance much higher external magnetic field is needed. This seems to be the case with un-doped InSb films.

Figure 5.12(b) shows the magnetoresistance ratio versus applied magnetic field spectra for $In_{0.95}Mn_{0.05}Sb$ film at different temperature. The MR spectra (**figure 5.12(b)**) of the $In_{0.95}Mn_{0.05}Sb$ film show that the maximum variation in magnetoresistance is 4.7 % at 20 K with 5 tesla applied magnetic field.
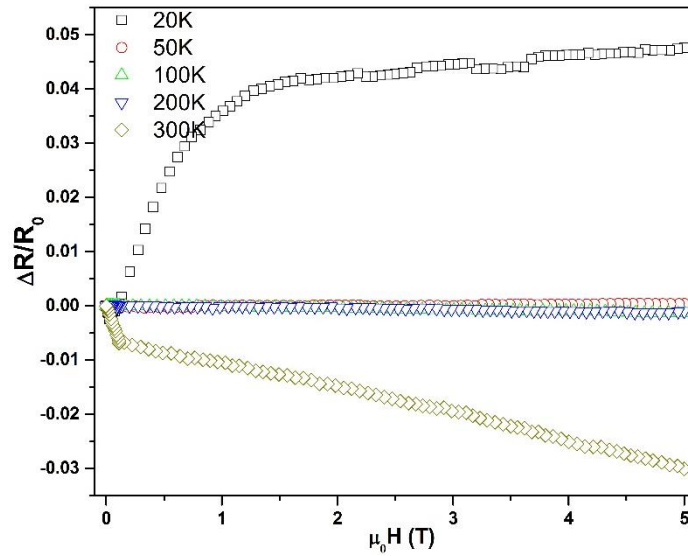

Figure 5.12(b): Magnetoresistance ratio (ΔR/R) versus magnetic field of the $In_{0.95}Mn_{0.05}Sb$ film at different temperature

This variation of magnetoresistance in $In_{0.95}Mn_{0.05}Sb$ film at 20 K is twice multiple as compared to the un-doped InSb film. At higher temperatures till 200 K there is no significant change observed for $In_{0.95}Mn_{0.05}Sb$ film. At ~ 300 K temperature negative magnetoresistance ratio is observed with the MR ratio variation of -3.2 %. In some of the earlier studies by Oiwa *et. al.* **[64]** and Iye *et. al.* **[65]** they observed large negative magnetoresistance at low temperatures in the $Ga_{1-x}Mn_xAs/GaAs$ (x < 0.071) samples. They proposed the Anderson localization **[66-67]** for the explanation of the negative magnetoresistance in these samples. In the present study, a negative

magnetoresistance ratio is observed at RT. This may be explained in terms of the defects present in the films. As Mn is doped there is a possibility of Mn going to both substitutional, and interstitial sites in InSb lattice and in the process increasing the amorphization of the films as is evident from XRD. The defect induced changes take place in the magnetization. This corresponds to a change in spin disorder which is related to resistivity. Also magnetic inhomogeneity can give rise to dramatic change in magnetoresistance. The electrons in the interstitial sites are more mobile as compared to the one at substitutional sites. At RT, these electrons in presence of the external field become more mobile and show negative MR. It is also possible that if the temperature is further increased, this effect may get more pronounced. This scenario seems to be the case in Mn doped InSb film.

The magnetoresistance variation ratio versus applied magnetic field of $In_{0.95}Ni_{0.05}Sb$ film is shown in **figure 5.12(c)**.

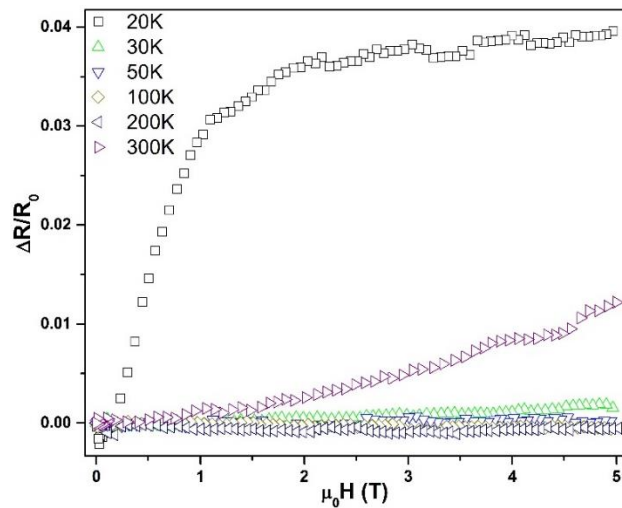***Figure 5.12(c):** Magnetoresistance ratio (ΔR/R) versus magnetic field of the $In_{0.95}Ni_{0.05}Sb$ film at different temperature*

The $In_{0.95}Ni_{0.05}Sb$ film grown on Si substrate shows the MR variation of 4.0 % with applied magnetic field of 5 tesla at 20 K temperature. The MR variation ratio is observed to be saturated (become constant) with the increase in applied magnetic field

after 2.5 tesla at 20 K. The temperature between $20 < T < 300$ K, there is no significant change in MR ratio with increase in magnetic field. At RT (~ 300 K) 1.3 % MR ratio variation is observed in the magnetic field of 5 tesla. This change in the MR ratio linearly increases with the increase in applied magnetic field at 300 K. It can be seen on comparison of the XRD spectra of Ni doped InSb film the crystalline nature of the film increases as compared to un-doped and Mn doped InSb film. The chances of Ni going to substitutional site having a charge state of Ni^{2+} are more as compared to interstitial sites in InSb matrix at Indium site. As Ni is confined in the matrix there is no change in magnetoresistance till 200 K. It seems to have an effect on magnetoresistance more magnetic field is required. At lower temperatures the effect of the magnetic field increase is not able to have any effect on the confined electrons and hence no change in magnetoresistance. The other way of compensating for this confinement of electrons is to increase the temperature. It seems that at RT, the energy of these electrons becomes more and hence is able to respond to the applied magnetic field. Also, these confined electrons respond less to external magnetic field; hence the positive magnetoresistance ratio is seen to increase with the external field. The conductance measurement also supports this argument.

Figure 5.12(d) shows the magnetoresistance ratio versus applied magnetic field spectra for Fe doped InSb film at different temperature. From this figure it is observed that MR ratio variation in $In_{0.95}Fe_{0.05}Sb$ at 5 K temperature is maximum and it is observed to be ~ 0.055 % at an applied magnetic field of 5 tesla. The observed MR ratio variation decreases with the increase in temperature from 5 K to 200 K. Fe seems to be in a mixed valence state of +2 and +3.
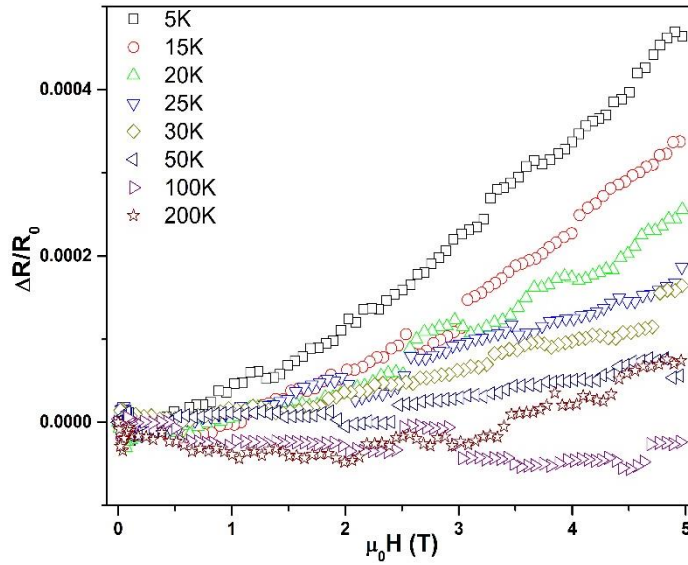
Figure 5.12(d): *Magnetoresistance ratio (ΔR/R) versus magnetic field of the In$_{0.95}$Fe$_{0.05}$Sb film at different temperature.*

Due to the mixed valence state as the no. of electrons increases resulting in the conductivity to increase with temperature. This is also corroborated by the resistivity-temperature study. The MR curve shows that with an increase in temperature the MR ratio decreases. At 20 K, 1 tesla field, in comparison to un-doped InSb film, the Fe doped InSb film shows the extremely low MR ratio of 0.003%. This seems to be due to increases in charge density in a given area of film. As a result of large repulsion, the mobility of the electrons increases compared to un-doped film. Even a low intensity field can realign the electrons in the direction of the field. Hence increase in the MR ratio with an increase in intensity of magnetic field at a constant temperature. With increase in temperature the temperature effect also plays its role in decreasing the MR ratio as observed in Fe doped InSb film.

5.2.6   Surface studies

For the surface morphology atomic force microscopy technique is used on un-doped and In$_{0.95}$M$_{0.05}$Sb (M = Mn, Fe, Co and Ni) films.
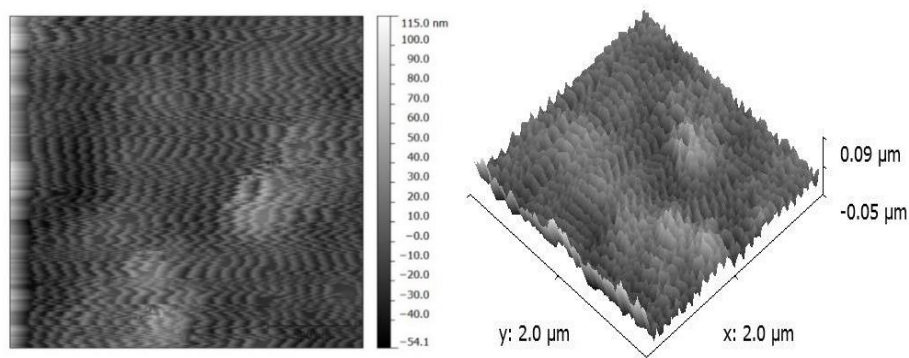
Figure 5.13(a): 2-D and 3-D AFM image of un-doped InSb film grown at Silicon substrate
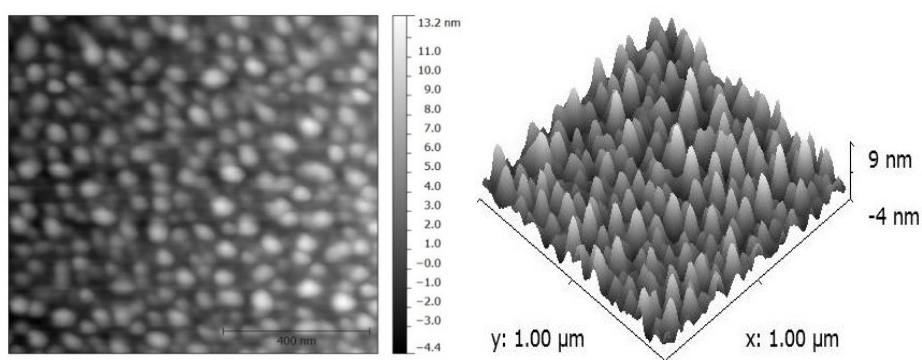

Figure 5.13(b): 2-D and 3-D AFM image of $In_{0.95}Mn_{0.05}Sb$ film grown at Silicon substrate
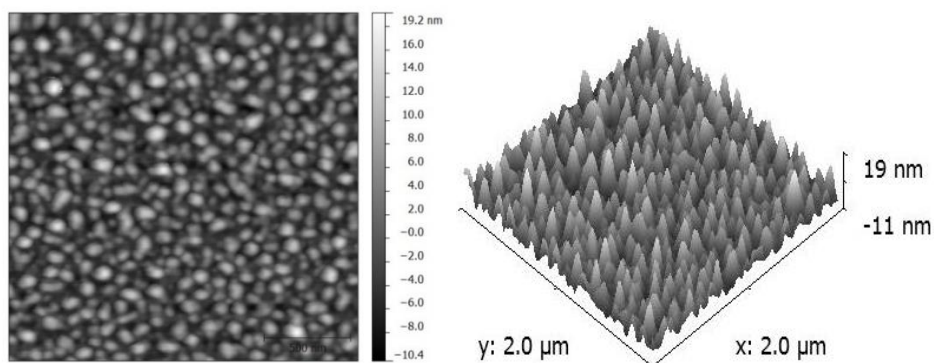

Figure 5.13(c): 2-D and 3-D AFM image of $In_{0.95}Fe_{0.05}Sb$ film grown at Silicon substrate

Figure 5.13(a-e) shows the two dimensional (left side) and corresponding three dimensional (right side) AFM images of un-doped InSb and $In_{0.95}M_{0.05}Sb$ (M = Mn, Fe, Co and Ni) films grown on Silicon substrate respectively.
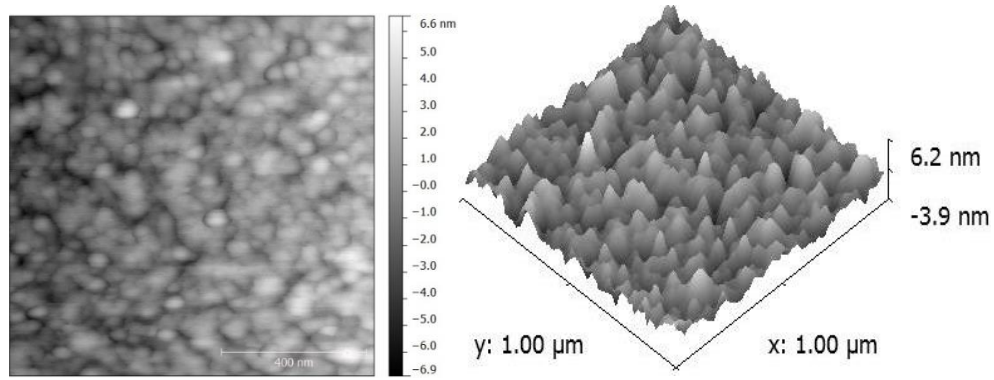
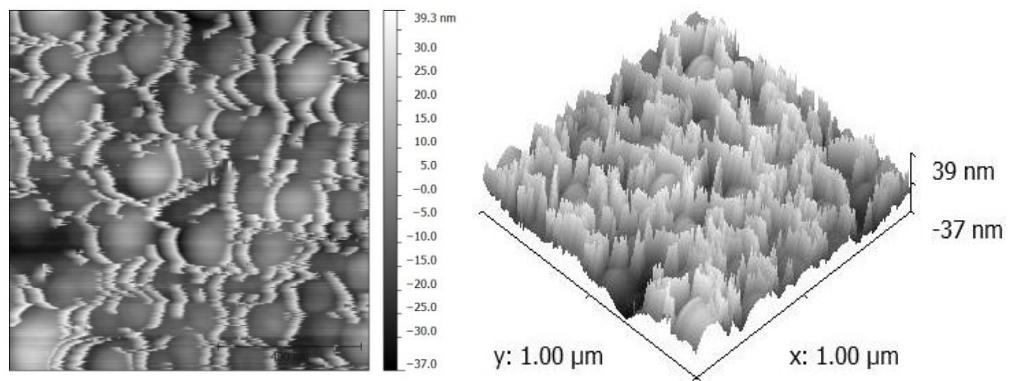*Figure 5.13(d):* 2-D and 3-D AFM image of In$_{0.95}$Co$_{0.05}$Sb film grown at Silicon substrate

Figure 5.13(e): 2-D and 3-D AFM image of In$_{0.95}$Ni$_{0.05}$Sb film grown at Silicon substrate

The AFM images of un-doped and doped with transition metal shows that particles are distributed evenly on the surface of the films. The AFM studies reveal that the root means squared (rms) roughness decreases with doping of TM as compare to un-doped film. The rms roughness for TM doped films is in the range of 2- 13 nm while for un-doped film it is 18.27 nm. The height of the maximum available peak and average available peak is determined using histogram analysis. The roughness histogram for un-doped and In$_{0.95}$M$_{0.05}$Sb (M = Mn, Fe, Co and Ni) films are shown in **figure 5.14(a-e)** respectively. The average peak height and maximum peak height of TM doped films also decreases as compare to un-doped InSb film.

Sample	rms roughness (nm)	Average peak height (nm)	Maximum peak height (nm)
InSb	18.27	50.62	82.57
$In_{0.95}Mn_{0.05}Sb$	02.06	05.12	07.86
$In_{0.95}Fe_{0.05}Sb$	04.41	10.39	28.55
$In_{0.95}Co_{0.05}Sb$	01.20	04.34	9.62
$In_{0.95}Ni_{0.05}Sb$	13.13	35.90	66.89

Table 5.5: *Microstructural parameters calculated from atomic force microscope (AFM)*
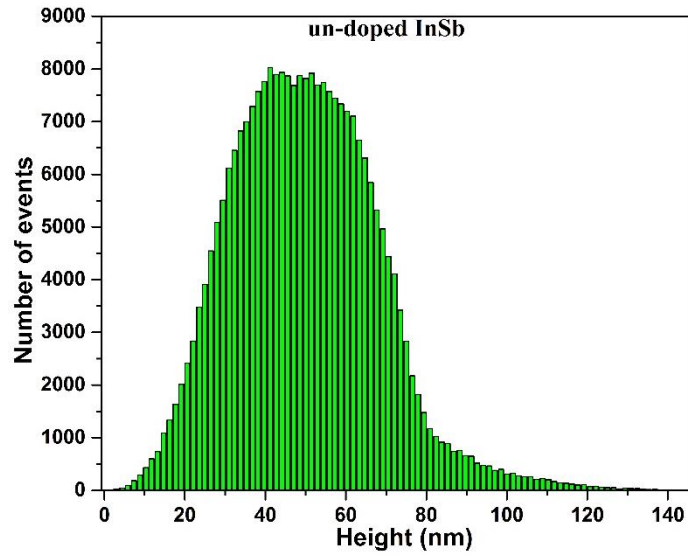

Figure 5.14(a): *Roughness histogram showing peak height statistics for Un-doped InSb film grown at Si substrate*
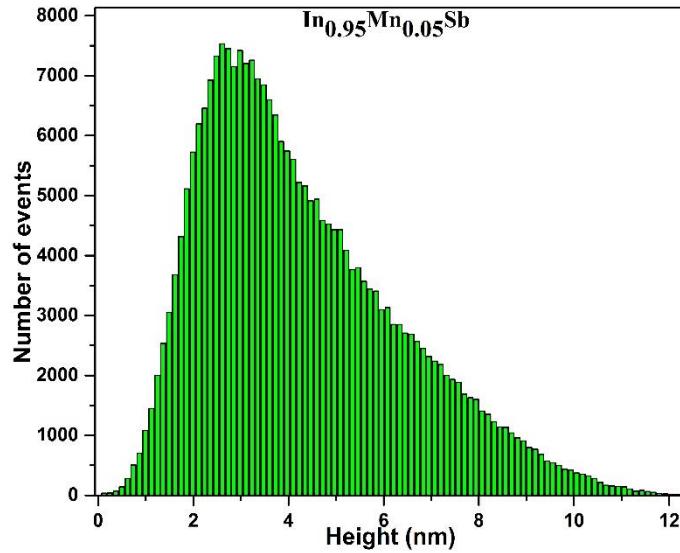

Figure 5.14(b): *Roughness histogram showing peak height statistics for $In_{0.95}Mn_{0.05}Sb$ film grown at Si substrate*

For the TM doped films the average peak height and maximum peak height are in the range of ~ 5- 35 and ~ 7- 66 nm respectively. While the average peak height and maximum peak height for un-doped film is ~ 50 nm and ~ 82 nm respectively.
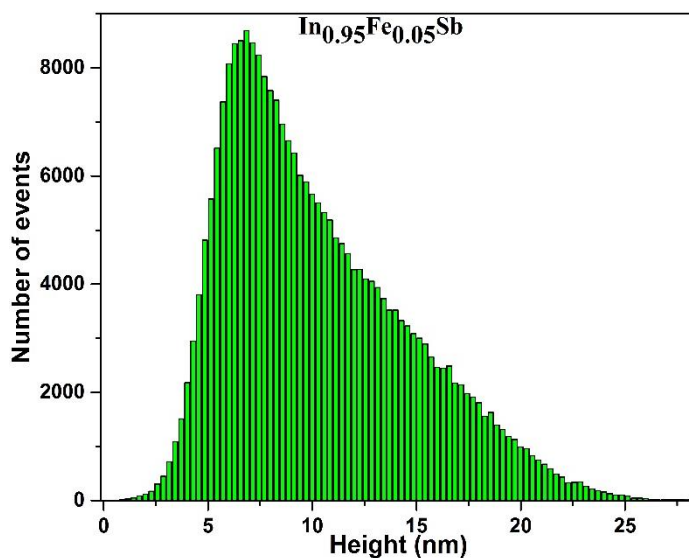

Figure 5.14(c): *Roughness histogram showing peak height statistics for In$_{0.95}$Fe$_{0.05}$Sb film grown at Si substrate*
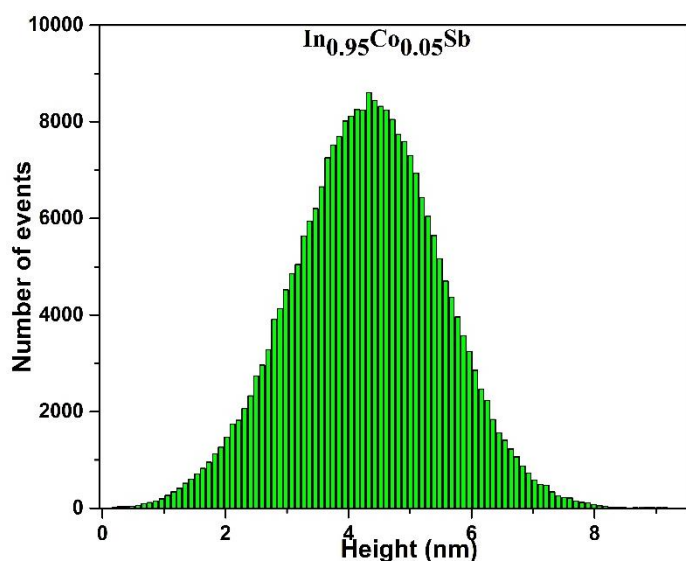
Figure 5.14(d): *Roughness histogram showing peak height statistics for In$_{0.95}$Co$_{0.05}$Sb film grown at Si substrate*

The lowest rms roughness, average peak height and maximum peak height are observed for In$_{0.95}$Mn$_{0.05}$Sb film and it is maximum for In$_{0.95}$Ni$_{0.05}$Sb film respectively. The value of rms roughness, average peak height and maximum peak height for un-doped and In$_{0.95}$M$_{0.05}$Sb (M = Mn, Fe, Co and Ni) film is given in **table 5.5**.

Figure 5.14(e): *Roughness histogram showing peak height statistics for In$_{0.95}$Ni$_{0.05}$Sb film grown at Si substrate*
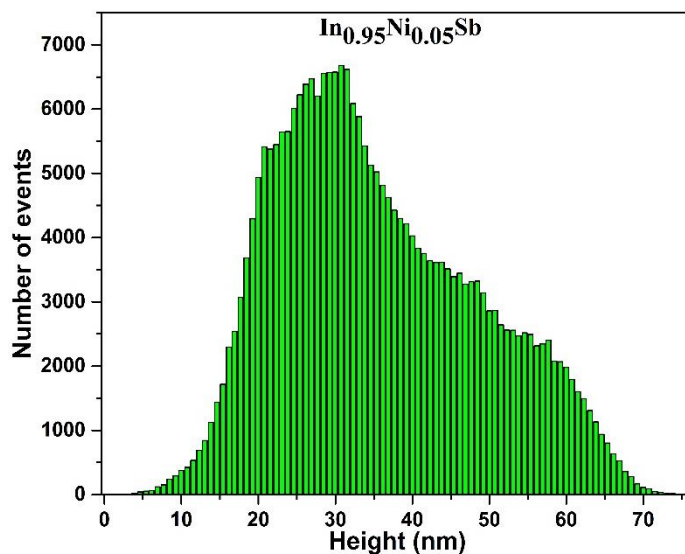
5.2.7 MFM studies

The magnetic force microscopy study is carried out to observe the comparative magnetic interactions at the surface of different TM doped InSb films. The **figure 5.15(a-e)** shows topography AFM images (left side) and corresponding MFM images (right side) of the un-doped and In$_{0.95}$M$_{0.05}$Sb (M = Mn, Fe, Co and Ni) films respectively. The MFM images are performed with atomic force microscope operating in tapping/lift mode, which combine interaction and constant height mode in order to separate short range topography and magnetic signals **[68-69]**.

Figure 5.15(a): *AFM (left side) and corresponding MFM image (right side) of un-doped InSb film grown on Silicon substrate*

Figure 5.15(b): AFM (left side) and corresponding MFM image (right side) of $In_{0.95}Mn_{0.05}Sb$ film grown on Silicon substrate.
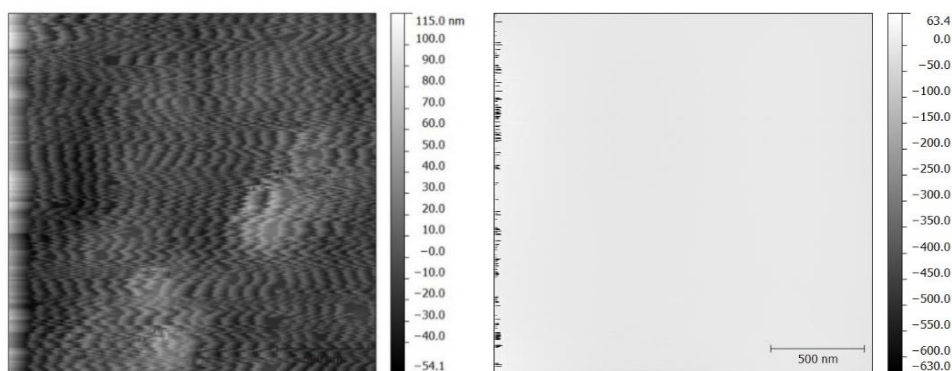

Figure 5.15(c): AFM (left side) and corresponding MFM image (right side) of $In_{0.95}Fe_{0.05}Sb$ film grown on Silicon substrate

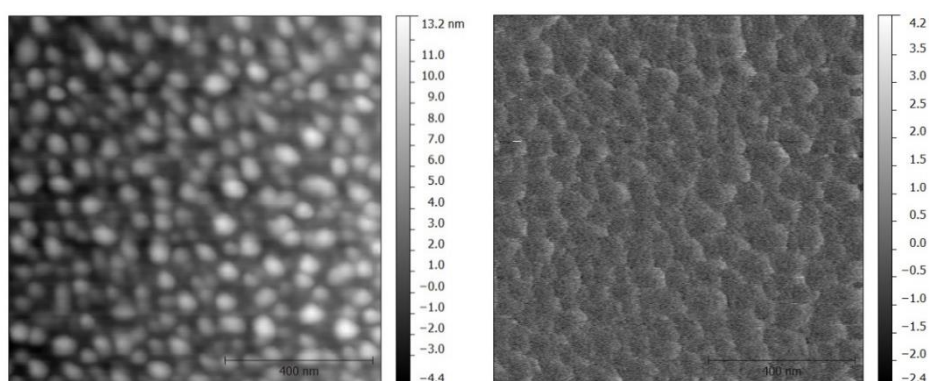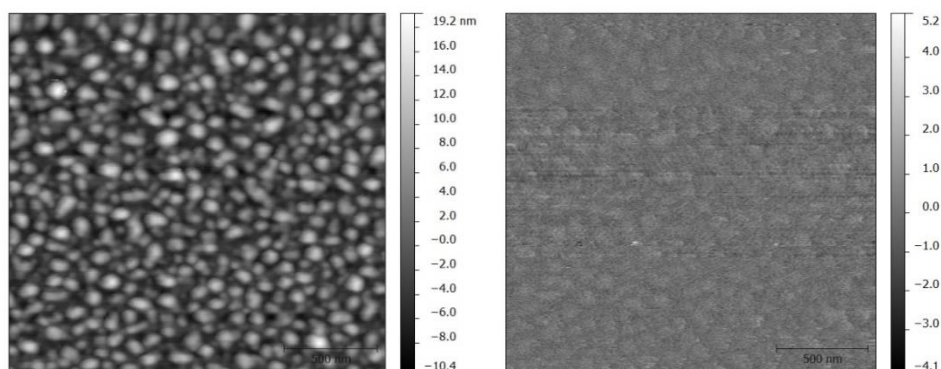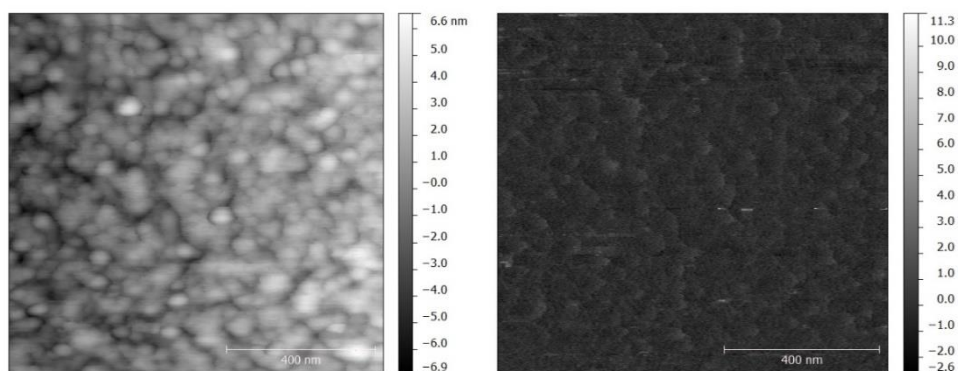*Figure 5.15(d): AFM (left side) and corresponding MFM image (right side) of $In_{0.95}Co_{0.05}Sb$ film grown on Silicon substrate*

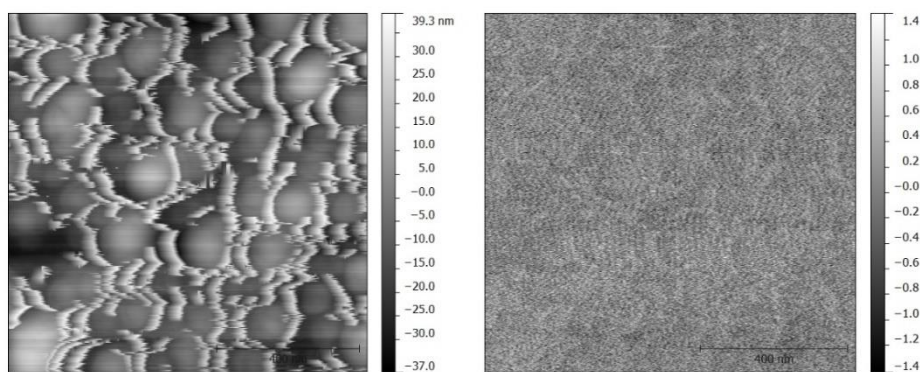*Figure 5.15(e): AFM (left side) and corresponding MFM image (right side) of In$_{0.95}$Ni$_{0.05}$Sb film grown on Silicon substrate*

For the comparative study of magnetic interactions with different TM doping in InSb films MFM studies are done. **Figure 5.15(a)** shows the AFM image (left side) and corresponding MFM image (right side) of un-doped InSb film. The MFM image shows that there is no magnetic interaction in un-doped film. **Figure 5.15(b)** shows the AFM (left side) and MFM (right side) image of In$_{0.95}$Mn$_{0.05}$Sb film. The AFM and MFM image differ in contrast respectively, which appears to decorate the topology. It is observed that in In$_{0.95}$Mn$_{0.05}$Sb film magnetic contrast is visible. It can also be seen that the magnetic domains are uniformly distributed in In$_{0.95}$Mn$_{0.05}$Sb film. **Figure 5.15(c)** shows the AFM and corresponding MFM image of In$_{0.95}$Fe$_{0.05}$Sb film. The AFM and MFM images differ in contrast. This difference in contrast depicts that there is magnetic interaction at the surface of film. The weak contrast indicates weak interaction. It also shows the absence of clusters of Fe or Fe related any phase with InSb film. **Figure 5.15(d)** shows the AFM and corresponding MFM image of In$_{0.95}$Co$_{0.05}$Sb film. This MFM image shows the uniform distribution of magnetic interaction over all the film. The MFM image of the Co doped InSb film reveals there is a weak contrast of MFM image to indicating the absence of the Co or Co related clusters and any magnetic phase of Co. **Figure 5.15(e)** shows the AFM and MFM image of the Ni doped InSb film. Also,

a weak magnetic interaction is observed in the MFM image of the Ni doped InSb film. The distribution of magnetic regions is uniform.

5.2.8   Magnetic studies

The DC magnetization M, is investigated with an MPMS SQUID- Vibrating Sample magnetometer (VSM) system. It provides faster and accurate DC-magnetization measurements, especially for films. In the SQUID VSM measurement technique, the sample vibrates at a known frequency and the SQUID detection system is employed for signal detection [70]. The measurement is performed in the temperature range of 4-300 K in the magnetic field up to 6 tesla. This magnetization measurement is performed for $In_{0.95}Fe_{0.05}Sb$, $In_{0.95}Mn_{0.05}Sb$ and $In_{0.95}Co_{0.05}Sb$ film. The magnetic moment as a function of temperature (M-T) is performed to observe the magnetic transition temperature as well as to observe the magnetic nature of the film at different temperatures. There are two ways of doing this measurement. In the first case the sample is cooled up to 4 K without applying a magnetic field. After reaching the desired temperature a field of 100 Oe is applied and the sample is heated from 4 K-300 K and the change in the magnetic moment versus temperature is measured. This cycle is called zero field cooling (ZFC). Secondly, the sample is cooled in the presence of some applied field (as 100 Oe) down to 4 K temperature and again the magnetic moment versus temperature is measured by increasing the temperature from 4 K to 300 K in the presence of the same field. This cycle is called field cooling cycle (FC).

The magnetization versus applied magnetic field curve "M(B)" is investigated with the applied field variation of 6 tesla.
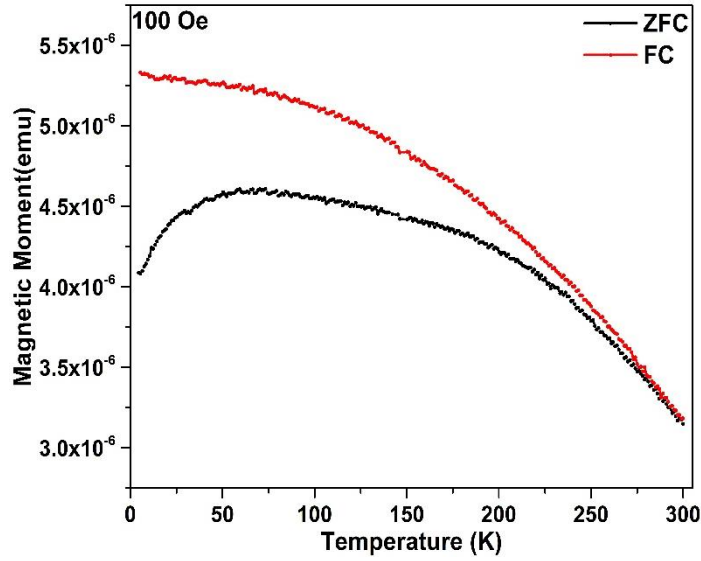
Figure 5.16(a): *Temperature dependence of magnetization curve (M-T curve) for In$_{0.95}$Fe$_{0.05}$Sb film. The black curve shows the zero field cooling (ZFC) and red curve shows the field cooling (FC). The M-T curve is taken at the field of 100 Oe*

The magnetic moment versus temperature variation is measured as the temperature is increased from 4 to 300 K **[71]**. **Figure 5.16(a)** shows the magnetization versus temperature curve for zero field cooling (ZFC) and field cooling (FC) measurement for In$_{0.95}$Fe$_{0.05}$Sb film. The ZFC magnetization curve increases as low temperature, reaching a maximum at temperature ~65 K having magnetic moment value of 4.602×10^{-6} emu. The FC curve increases as the temperature decreases and never reaches saturation at low temperature. Beyond the temperature of ~65 K magnetization value of ZFC and FC curve decreases with the rise in temperature gradually.

The ZFC curve in **figure 5.16(a)** shows the antiferromagnetic to paramagnetic transition at ~ 25 K. The Fe doped InSb film shows antiferromagnetic nature below 25 K and above that temperature the film shows paramagnetic nature. The magnetic moment does not drop to zero, suggesting a high Curie temperature beyond RT.
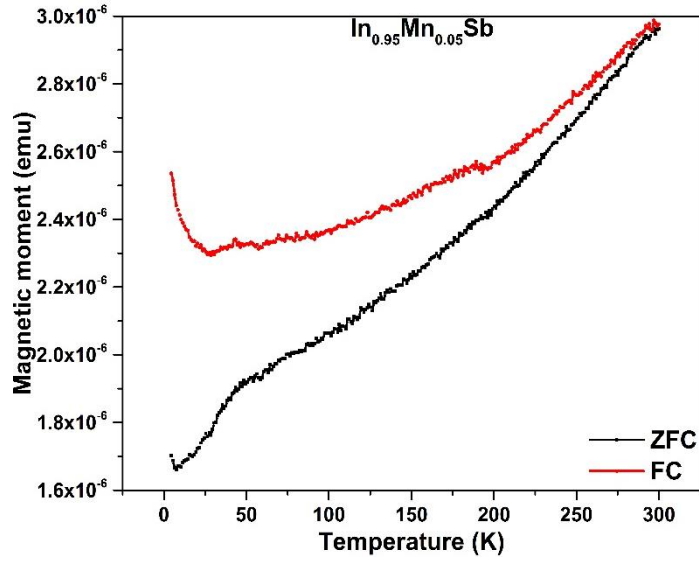
Figure 5.16(b): *Temperature dependence of magnetization curve (M-T curve) for In$_{0.95}$Mn$_{0.05}$Sb film. The black curve shows the zero field cooling (ZFC) and red curve shows the field cooling (FC). The M-T curve is taken at the field of 100 Oe*
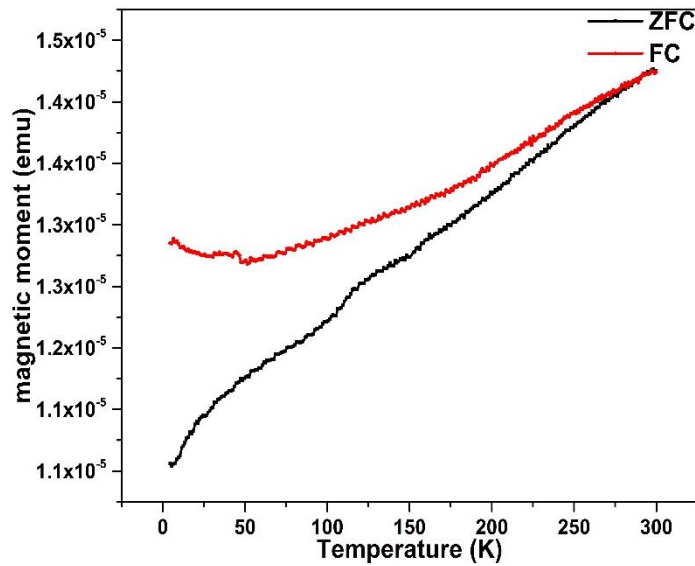
Figure 5.16(c): *Temperature dependence of magnetization curve (M-T curve) for In$_{0.95}$Co$_{0.05}$Sb film. The black curve shows the zero field cooling (ZFC) and red curve shows the field cooling (FC). The M-T curve is taken at the field of 100 Oe*

The ZFC and FC curve starts to split below 275 K and a divergence between the ZFC and FC increases with decreasing the temperature. As the temperature decreases below ~ 70 K, the FC magnetization value increases with decrease in temperature while ZFC magnetization drastically decreases with the temperature. These results indicate

149

that there is a change in spin ordering at low temperature, may be due to spin reorientation in $In_{0.95}Fe_{0.05}Sb$ film.

Figure 5.16(b) displays the ZFC and FC magnetizations of the $In_{0.95}Mn_{0.05}Sb$ film. The magnetization as a function of temperature is performed by an external applied field of 100 Oe. The DC magnetization (ZFC and FC) curves are recorded in a temperature range of 4 to 300 K. The magnetization value of ZFC and FC decreases with decrease in temperature from 300 to 50 K, which is consistent with the conventional antiferromagnetic nature of $In_{0.95}Mn_{0.05}Sb$ film. It is also observed in the ZFC and FC curve of $In_{0.95}Mn_{0.05}Sb$ film that the two curve starts to split below 290 K and the divergence between the ZFC and FC increases with decrease in temperature. As the temperature decreases below ~ 50 K, FC magnetization increases with the decrease in temperature while ZFC magnetization almost linearly decreases with decrease in temperature. This decrease in magnetic moment for ZFC shows the contribution of the super paramagnetic particles to the resultant moment. The linear decrease in ZFC curve with temperature suggests the amorphization of the films.

The ZFC magnetization in this film decreases to a minima at a temperature ~25 K and suddenly starts to increase as the temperature is further decreased. These results indicate that at ~25 K, there is a spin fluctuation at low temperature and spin reorientation takes place in $In_{0.95}Mn_{0.05}Sb$ film. The magnetization ZFC and FC curve of $In_{0.95}Co_{0.05}Sb$ is shown in **figure 5.16(c)**. The same kind of phenomenon also occurs in the $In_{0.95}Co_{0.05}Sb$ film. The only difference is in Co doped system is there seems to be less strain as compared to Mn doped system. This could be due to less number of unpaired electrons in Co doped system as compared to Mn doped system in which Mn seems to be in mixed valence state. Hence the effect near 25K is more pronounced in Mn doped InSb film as compared to Co doped Film.
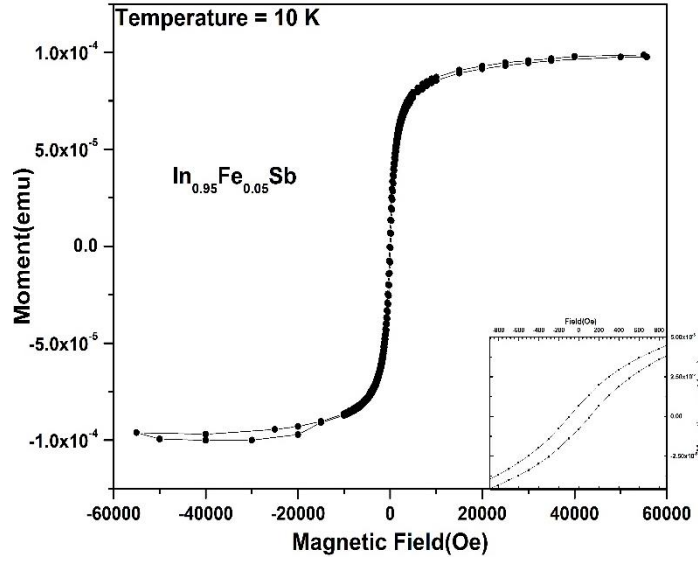
Figure 5.17: *Hysteresis curve recorded at 10 K for $In_{0.95}Fe_{0.05}$Sb film, inset: zoom of the hysteresis cycle at low fields*

This splitting of the ZFC and FC curves in $In_{0.95}M_{0.05}$Sb (M = Fe, Mn and Co) may be appearing due to the co-existent system of antiferromagnetic and ferromagnetic phases [72-73]. This splitting of ZFC and FC magnetization at low temperature also reveals spin glass transition in $In_{0.95}M_{0.05}$Sb (M = Fe, Mn and Co) films grown at Silicon substrate [74].

Figure 5.17 shows the magnetic moment versus applied magnetic field (H) curve (M-H curve) of $In_{0.95}Fe_{0.05}$Sb film at 10 K temperature. The figure shows the hysteresis behavior of $In_{0.95}Fe_{0.05}$Sb film. The value of coercivity and the residual magnetization is found to be ~ 100 Oe and 6.8811 emu respectively from the hysteresis curve of $In_{0.95}Fe_{0.05}$Sb (**figure 5.17**) film.

References

[1]. V.M. Goldschmidt *Transactions of the Faraday Society* **25** 253-83 (1929).

[2]. T.S. Liu and E.A. Peretti *Transactions of the American Society of Metals* **44** 539-45 (1952).

[3]. B.V. Rao, D. Gruznev, T. Tambo and C. Tatsuyama *Semicon. Sci. Technol.* **16** 216 (2001).

[4]. R. A Stradling *Braz. J. Phys.* **26** 7 (1996).

[5]. K. Kanisawa, H. Yamaguchi and Y. Hirayama *Appl. Phys. Lett.* **76** 589 (2000).

[6]. Gert Finger, Reinhold J. Dorn, Manfred Meyer, Leander Mehrgan, Jorg Stegmeier and Alan Moorwood *Nucl. Instr. and Meth A.* **549** 79 (2005).

[7]. Atsushi Okamoto, Takashi Yoshida, Shogo Muramatsn and Ichiro Shibasaki *J. Cryst. Growth* **201** 765 (1999).

[8]. S. Ozer and Besikci *J. Phys. D: Appl. Phys.* **36** 559 (2003).

[9]. K.F. Hulme and J.B. Mullin *Solid-State Electronics* **5** 211–247 (1962).

[10]. S.C. Liang, R.K. Willardson and H.L. Goering Eds *Rheinhold Publishing, New York* **1** (1962).

[11]. M. Neuberger NTIS ADA **47667S** 1-201 (1965).

[12]. M. Neuberger New York-Washington-London: IFI/Plenum 77–92 (1971).

[13]. J. Camassel and D. Auvergne *Phys. Rev. B* **12(8)** 3258 (1975).

[14]. W.F.H. Micklethwaite *John wiley & sons* Ltd. ISBN: 978-0-470-85142-5.

[15]. P. Mohan et. al. *J. Cryst. Growth* **200** 96-100 (1999).

[16]. D. S. Maske et. al. *Arch. Phy. Res.* **3 (1)** 15-20 (2012).

[17]. D. B. Gadkari *Indian J. Pure Appl. Phys.* **38** 237-242 (2000).

[18]. Robert D. Grober et. al. *J. Appl. Phys.* **71** 10 (1992).

[19]. A. A. Ebnalwaled et. al. *J. Cryst. Growth* **311** 4385-90 (2009).

[20]. A. A. Ebnalwaled International journal of Basic & applied sciences 11 194 (2011).

[21]. K. E. Hnida et. al. *J. Mater. Chem. C.* **4** 1345 (2016).

[22]. D. B. Gadkari, K. B. Lal, A. P. Shah, B. M. Arora *J. Cryst. Growth* **173** 585-588 (1997).

[23]. Shigeo Yamaguchi, Takayuki Matsumoto, Jun Yamazaki, Nakaba Kaiwa, and Atsushi Yamamoto *Appl. Phys. Lett.* **87** 201902 (2005).

[24]. Manisha Joshi Deshpande, Dilip Maske, BrijMohan Arora, Dattatray Gadkari *Internationl journal of Scientific and research publications* **4** 1-3 (2014).

[25]. V. A. Ivanov and O. N. Pashkova et. al. *Inorganic materials* **44** 1041-46 (2008).

[26]. Kochura et. al. *J. Appl. Phys.* **113** 083905 (2013).

[27]. E. Lahderanta et. al. *Phys. Status Solidi A* **1** 8 (2014).

[28]. D. L. Williamson, L. Niesen, G. Weyer, R, Sielemann and G. Langouche *Hyperfine interactions of defects in semiconductors* (Elsevier, Amsterdam, 1992) pp. 1ff.

[29]. Th. Wichert, N. Achtziger, H. Metzner and R. Sielemann *Hyperfine interactions of defects in solids* (Elsevier, Amsterdam, 1992) pp. 79ff.

[30]. R. Mariappan, V. Ponnuswamy, P. Suresh, R. Suresh, M. Ragavendar and C.Sankar *Materials Science in Semiconductor processing* **16** 825 (2013).

[31]. G. K. Williamson and W. H. Hall *Acta Matell.* **1** 22 (1953).

[32]. A. Khorsand Zak, W. H. Abd. Majid, M. E. Abrishami and Ramin Yousefi *Solid state Sciences* **13** 251 (2011).

[33]. J. I. Chyi, D. Biswas, S. V. Iyer, N. S. Kumar, H. Morkox, R. Bean, K. Zanio, R. Grober and D. Drew *J. Vac. Sci. Technol. B* **7** 345 (1989).

[34]. Gert Finger, Reinhold J. Dorn, Manfred Meyer, Leander Mehrgan, Jorg Stegmeier and Alan Moorwood *Nucl. Instr. and Meth A.* **549** 79 (2005).

[35]. Orias. G, Hoffman A. W and Casselman M. F. *SPIE J.* **627** 408 (1986).

[36]. J. B. Webb and C. Halpren *Appl. Phys. Lett.* **47** 831 (1985).

[37]. P. k. Chang and S. M. Bedair *Appl. Phys. Lett.* **46** 383 (1985).

[38]. E Michel., J Xu, J. D Kim, I Ferguson and M Razeghi. *IEEE Phot. Tech. Lett.* **8** 673 (1996).

[39]. A. Rogalski *Infrared Phys. Technol.* **43** 187 (2002).

[40]. G. E. Franklin, D. H. Rich, Hong Hawoong, T. Miller and T. C. Chiang *Phy. Rev. B* **45** 3426 (1992).

[41]. B.V. Rao, Atoji. M, Li D M, Okamoto. T, Tambo. T and C Tatsuyama *Jap. J. Appl. Phys.* **37** L1297 (1998).

[42]. M. Mori, M. Saito, K. Nagashima, K. Ueda, T. Yoshida, and K. Maezawa *J. Cryst. Growth* **311(7)** 1692 (2009).

[43]. S A Obukhov, B S Neganov, Yu F Kiselev, A N Chirnikov, V S Vekshina, N I Pepik and A N popkov *cryogenics* **31** 874 (1991).

[44]. M Y dashevskii, V S Ivleva, L Y Krol, I N Kurilenko, L B Litvak- Gorskaya, R S Mitrofanova and E Y fridlyand *Sov. Phys. Semicond.* **5** 757 (1971).

[45]. J. Teubert, S A Obukhov, P J klar and W Heimbrodt *Phys. Rev. Lett.* **102** 046404 (2009).

[46]. D L partin, J Heremans and C M Thrush *J. cryst. Growth* **175** 860 (1997).

[47]. V. M. Novotortsev, I. S. Zakharov, A. V. Kochura, S. F. Marenkin, R. Laiho, E. Lahderanta, A. Lashkul, A. G. Veresov, A. V. Molchanov, and G. S. Yur'ev *Russian Journal of Inorganic Chemistry* **51** 10 (2006).

[48]. E. S. Demidov, V. V. Podol'skii, V. P. Lesnikov, M. V. Sapozhnikov, D. M. Druzhnov, S. N. Gusev, B. A. Gribkov, D. O. Filatov, Yu. S. Stepanova, and S. A. Levchuk *Journal of Experimental and Theoretical Physics* **106** 110 (2008).

[49]. T. Wojtowicz et. al. *Appl. Phys. Lett.* **82** 4310 (2003).

[50]. T Wojtowicz et. al. *Physica E* **20** 325 (2003).

[51]. S. Yanagi, K Kuga, T Slupinski and H Munekata *Physica E* **20** 333 (2004).

[52]. J Hollings wort and P R Bandaru *Materials Science and Engineering B* **151** 152 (2008).

[53]. Yu A Danilov, E S Demidov, Yu N Drosdov, V P Lesnikov, V V Podolski, M V Sapozhnikov and A P Kasatkin *J. Magn. Magn. Mater.* **300** 24 (2006).

[54]. V A Ivanov, O N Pashkova, E A Ugolkova, V P Sanygin and R M Galera *Inorganic Materials* **44** 1041 (2008).

[55]. Y.X. Chen, Shi Shen Yan, Y. Fang, Y.F. Tian, S.Q. Xiao, G.L. Liu, Y.H. Liu, L.M. Mei *Appl. Phys. Lett.* **90** 052508 (2007).

[56]. Vinay Ambegaokar, B.I. Halperin, J.S. Langer *Phys. Rev. B* **8** 4 (1971).

[57]. Shubra Singh, M. S. Ramchandra Rao *Phys. Rev. B* **80** 045210 (2009).

[58]. Stephen Blundell, Magnetism in condensed matter, Oxford master series in condensed matter physics, Oxford University press (2001).

[59]. G. S. Nadkarni and A. Simoni *Solid-st. Electron.* **18** 393-97 (1975).

[60]. H. H. weider *Solid-St. Electron* **9** 373 (1966).

[61]. J. A. Carroll and J. F. Spivak *Solid-St. Electron* **9** 383 (1966).

[62]. H. H. Weider *J. Appl. Phys.* **40** 3320 (1969).

[63]. N. F. Teede *Solid-St. Electron* **10** 1069 (1967).

[64]. A. Oiwa, S. Katsumoto, A. Endo, M. Hirasawa, Y. Iye, H. Ohno, F. Matsukura, A. Shen, and Y. Sugawara *Phys. Status solidi (b)* **205(1)** 167 (1998).

[65]. Y. Iye, A. Oiwa, A. Endo, S. Katsumoto, F. Matsukura, A. Shen, H. Ohno, and H. Munekata *Mater. Sci. Eng. B* **63** 88–95 (1999).

[66]. D. J. Thouless *J. Phys. C* **3** 1559 (1970).

[67]. P. W. Anderson. *Proc. Nat. Acade. Sci. USA* **69** 1097–1099 (1972).

[68]. S. Porthum, L. Abelmann and C. *J.* Lodder *Magn. Mater* **182** 238 (1998).

[69]. F. Singh, D. K. Awasthi, O. Angelov, P. Berthet, J. C. Pivin *Nucl. Instrum. Meth B* **245** 214-218 (2006).

[70]. Link http://www.csr.res.in/vsm_squid.html

[71]. X. X. Zhang, Magnetic relaxation and Quantum tunneling of Magnetization: Handbook of Advanced Magnetic materials, Tsinghu University press, New York (2005).

[72]. F. Z. Huang *et. al. Thin Solid films* **520** 6489 (2012).

[73]. Fengzhen Huang, Zhijun Wang, Xiaomei Lu, Junting Zhang, Kangli Min, Weiwei Lin, Ruixia Ti, TingTing Xu, Ju He, Chen Yue and Jinsong Zhu *Nature Scientific reports* **3** 2907 (2013).

[74]. Manoj K. Singh, W. Prellier, M. P. Singh, Ram S. Katiyar and J. F. Scott, *Phys. Rev. B* **77** 144403 (2008).